Lithos 318–319 (2018) 478–493

Contents lists available at ScienceDirect

Lithos

journal homepage: www.elsevier.com/locate/lithos

New geochemical constraints on the origins of MARID and PIC rocks: Implications for mantle metasomatism and mantle-derived potassic magmatism

Angus Fitzpayne [a,*], Andrea Giuliani [a,b], Janet Hergt [a], David Phillips [a], Philip Janney [c]

[a] KiDs (Kimberlites and Diamonds), School of Earth Sciences, The University of Melbourne, Parkville, 3010, Victoria, Australia
[b] ARC Centre of Excellence for Core to Crust Fluid Systems and GEMOC, Department of Earth and Planetary Sciences, Macquarie University, North Ryde, 2109, New South Wales, Australia
[c] Department of Geological Sciences, University of Cape Town, Rondebosch 7701, South Africa

ARTICLE INFO

Article history:
Received 18 May 2018
Accepted 29 August 2018
Available online 4 September 2018

Keywords:
MARID
Metasomatism
Lithospheric mantle
Ultramafic potassic magmatism

ABSTRACT

MARID (Mica-Amphibole-Rutile-Ilmenite-Diopside) and PIC (Phlogopite-Ilmenite-Clinopyroxene) rocks are unusual mantle samples entrained by kimberlites and other alkaline volcanic rocks. The formation of MARID rocks remains hotly debated. Although the incompatible element (for example, large ion lithophile element) enrichment in these rocks suggests that they formed by mantle metasomatism, the layered textures of some MARID samples (and MARID veins in composite xenoliths) are more indicative of formation by magmatic processes. MARID lithologies have also been implicated as an important source component in the genesis of intraplate ultramafic potassic magmas (e.g., lamproites, orangeites, ultramafic lamprophyres), due to similarities in their geochemical and isotopic signatures. To determine the origins of MARID and PIC xenoliths and to understand how they relate to alkaline magmatism, this study presents new mineral major and trace element data and bulk-rock reconstructions for 26 MARID and PIC samples from the Kimberley-Barkly West area in South Africa. Similarities between compositions of PIC minerals and corresponding phases in metasomatised mantle peridotites are indicative of PIC formation by pervasive metasomatic alteration of peridotites. MARID genesis remains a complicated issue, with no definitive evidence precluding either the magmatic or metasomatic model. MARID minerals exhibit broad ranges in Mg# (e.g., clinopyroxene Mg# from 82 to 91), which may be indicative of fractionation processes occurring in the MARID-forming fluid/melt. Finally, two quantitative modelling approaches were used to determine the compositions of theoretical melts in equilibrium with MARID rocks. Both models indicate that MARID-derived melts have trace element patterns resembling mantle-derived potassic magma compositions (e.g., lamproites, orangeites, ultramafic lamprophyres), supporting inferences that these magmas may originate from MARID-rich mantle sources.

1. Introduction

MARID (Mica-Amphibole-Rutile-Ilmenite-Diopside) rocks are coarse-grained, ultramafic, and ultrapotassic (4.0–9.5 wt% K_2O) in composition (Dawson and Smith, 1977; Waters, 1987a). They occur as discrete xenoliths, or vein assemblages in composite xenoliths, entrained by archetypal (Group I) kimberlites and orangeites (formerly known as Group II or micaceous kimberlites; e.g., Smith, 1983). Bulk-rock enrichments in large ion lithophile elements (LILE) and light rare earth elements (LREE) have led to suggestions that MARID rocks represent a possible end-member product of progressive mantle metasomatism (Grégoire et al., 2002; Waters, 1987a, 1987b; Waters and Erlank, 1988). MARID rocks have also been proposed as a major source of mantle-derived ultramafic potassic magmas including lamproites (Matchan et al., 2009), ultramafic lamprophyres (Tappe et al., 2008, 2017), kamafugites (Rosenthal et al., 2009), and orangeites (Giuliani et al., 2015). MARID rocks may also act as contaminants to magmas derived from the deeper, convective upper mantle (e.g., kimberlites), thereby causing significant shifts in their isotopic compositions (e.g., Tappe et al., 2011).

Grégoire et al. (2002) used mineral geochemical criteria to differentiate MARID rocks from a distinct type of strongly metasomatised, phlogopite-dominated mantle xenolith, which they termed 'PIC' (for its dominant mineralogy of Phlogopite-Ilmenite-Clinopyroxene). The majority of known MARID and PIC xenoliths originate from the Kimberley kimberlites (South Africa), although MARID samples have also been found in other southern African kimberlites (e.g., Letlhakane in the Magondi fold belt, and the Prieska region at the SW margin of the Kaapvaal craton; Field et al., 2008; Skinner et al., 1994; Stiefenhofer

* Corresponding author.
E-mail address: afitzpayne@student.unimelb.edu.au (A. Fitzpayne).

https://doi.org/10.1016/j.lithos.2018.08.036
0024-4937/

et al., 1997; Fig. 1), as well as in orangeites in the Barkly West area (e.g., Newlands and Roberts Victor: Dawson and Smith, 1977; Waters, 1987a, 1987b). The relative abundance of archetypal MARID rocks in the Kimberley kimberlites compared to other localities remains unexplained. Mantle metasomatism generating mica-amphibole-clinopyroxene-rich mantle lithologies (i.e. broadly mineralogically similar to MARID) occurs in many other locations (e.g., Germany and Uganda: Lloyd and Bailey, 1975; Canada: Peterson and le Cheminant, 1993; Tappe et al., 2006; Morocco: Wagner et al., 1996), but these rocks cannot be classified as MARID rocks because they do not display all of the following distinctive MARID characteristics:

1) The presence of K-richterite (as opposed to Ca-rich amphiboles);
2) Al-Cr-depletion of all silicate phases compared to peridotitic mineral compositions. This is most notable in phlogopite, wherein a significant amount of Fe substitutes for Al and Si into the tetrahedral site (e.g., Dawson and Smith, 1977); and
3) The absence of olivine coexisting with MARID phases.

The distinguishing features of MARID rocks can also be used to differentiate between MARID and PIC rocks. For example, PIC rocks do not contain K-richterite, and PIC minerals generally contain less FeO^T (i.e., total Fe expressed as FeO) than MARID minerals (i.e. PIC minerals have higher Mg#; Grégoire et al., 2002).

Despite several studies of the geochemistry of MARID xenoliths from South African localities, the genesis of these rocks remains unclear. MARID rocks may represent magmatic veins in the lithospheric mantle (Dawson and Smith, 1977; Jones et al., 1982; Waters, 1987a), which may be related to the crystallisation of orangeite magmas, based on trace element and Sr-Nd isotope evidence (e.g., Grégoire et al., 2002). This model may also require the fractionation of both olivine- and carbonate-rich components from the orangeite melt (Sweeney et al., 1993). The crystallisation of MARID rocks from a melt in the lithosphere

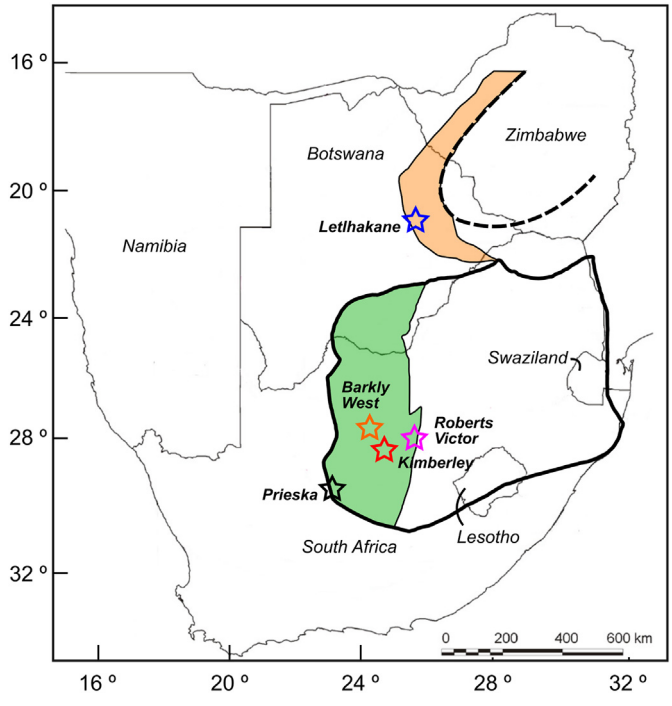

Fig. 1. A schematic map of southern Africa indicating the localities from which MARID rocks have previously been described; modified after Field et al. (2008). Thick black outline indicates the inferred boundary of the Kaapvaal craton; green shaded area depicts the craton's western terrane; thick dashed outline indicates the inferred boundary of the Zimbabwe craton; the orange shaded area depicts the Magondi fold belt.

may have led to the interaction of surrounding wall-rock with residual incompatible element-rich fluids, causing the adjacent peridotites to become metasomatised (e.g., Waters et al., 1989). Alternatively, MARID rocks may be formed by progressive metasomatic alteration of mantle peridotites (e.g., Sweeney et al., 1993). Erlank et al. (1987) described a metasomatic continuum from pristine garnet peridotite (GP), to garnet phlogopite peridotite (GPP) and phlogopite peridotite (PP), and finally to phlogopite K-richterite peridotite (PKP) based on petrography and mineral chemistry. According to Erlank et al. (1987), the development of phlogopite-K-richterite-rich rocks (including MARID) is the result of the most extensive metasomatism. However, owing to differences in mineral major element compositions in MARID and PKP samples, Erlank et al. (1987) proposed that the two could not be directly genetically related. Rocks belonging to the more recently defined PIC assemblage are suggested to form by extensive metasomatic alteration of peridotites by kimberlite melts, based on considerations of their trace element and radiogenic isotope compositions (Grégoire et al., 2002).

To provide new constraints on the genesis of MARID and PIC rocks, the compositions of their parental metasomatic fluids/melts, and the links between MARID and PIC rocks and ultramafic potassic magmas, we have examined the petrography and mineral major and trace element chemistry of 26 MARID and PIC xenoliths from southern African kimberlites and orangeites in the Kimberley and Barkly West areas (Fig. 1). "Reconstructed" bulk-rock compositions (calculated from modal and compositional data for primary minerals, thereby excluding secondary material in late stage veins and cracks) are presented and used to perform melting models of the unaltered MARID composition.

2. Geological setting

The xenolith samples used in the current study were collected from the Kimberley, Bultfontein, Wesselton, De Beers, and Kamfersdam kimberlites, and the Newlands orangeite, which are all located in or close to the town of Kimberley, in the Western terrane of the Kaapvaal craton (Field et al., 2008; Fig. 1). The Kimberley, Bultfontein, Wesselton, De Beers, and Kamfersdam pipes host archetypal kimberlite (Shee, 1985; Smith, 1983), whereas Newlands is an orangeite (e.g., Smith, 1983). The Kimberley kimberlites are younger (80–90 Ma; e.g., Allsopp and Barrett, 1975) than the Newlands orangeite (114 ± 1 Ma; Smith et al., 1985).

3. Samples and analytical methods

The 26 xenolith samples examined in this study were selected from a larger group of 40 xenoliths obtained from the collections housed in the John J. Gurney Upper Mantle Research Collection at the University of Cape Town, and the De Beers Consolidated Mines rock store. Additional samples were collected in 2015 and 2016 from the Boshof Road dumps, which host historical waste material from mining of the Bultfontein kimberlite. The samples vary from 5 to 15 cm in length. Samples for this study were chosen primarily on the basis of mineralogy, i.e. predominantly composed of phlogopite ± K-richterite ± clinopyroxene ± ilmenite ± rutile, with no obvious olivine, garnet, or orthopyroxene. Some of the selected samples (AJE-326; AJE-333; AJE-67; JJG-2040; JJG-2315; JJG-2327; JJG-2331) have been studied previously by Waters (1987a, 1987b).

Petrographic characterization of MARID and PIC samples was undertaken using a conventional petrographic microscope and a Philips (FEI) XL30 environmental scanning electron microscope (SEM), which was equipped with an OXFORD INCA EDS (energy dispersive X-ray spectrometer). Thin sections were scanned at very high resolution (>1200 DPI), following which point counting was performed on the scanned images using the JMicroVision image analysis toolbox (www.jmicrovision.com/index.htm, version 1.2.7, last accessed 13/03/2018). Major oxide compositions of minerals in thin section were obtained using a Cameca SX50 electron microprobe at the University of

Melbourne. The abundances of 38 trace elements in silicate and oxide minerals were measured in situ at the University of Melbourne, employing an Agilent 7700x quadrupole inductively coupled plasma mass spectrometer (ICP-MS) coupled to a custom-built RESOlution laser ablation system (constructed around a Compex 110 (Lambda Physik) ArF excimer laser), with a Laurin Technic S155 cell. Full analytical details for the collection of major and trace element compositions have previously been reported by Fitzpayne et al. (2018). The USGS BHVO-2G basaltic glass standard was used as the calibration material during laser ablation ICP-MS sessions. The isotopes ^{29}Si (phlogopite), ^{43}Ca (clinopyroxene and K-richterite), and ^{49}Ti (ilmenite and rutile) were employed as internal standards using nominal Si, Ca, and Ti concentrations determined by electron probe microanalysis (EPMA). The natural and synthetic glasses BCR-2G and NIST610 were also analysed as unknowns as a further measure of quality control, and returned values within 2 s.d. of published data (http://georem.mpch-mainz.gwdg.de/, last accessed on 05/04/2018; Jochum et al., 2011).

4. Petrography

Several samples examined in this study display massive textures (Fig. 2a), whereas others appear foliated due to the preferential orientation of mica grains. A few samples display modal layering of the main silicate minerals (typically of phlogopite and K-richterite or

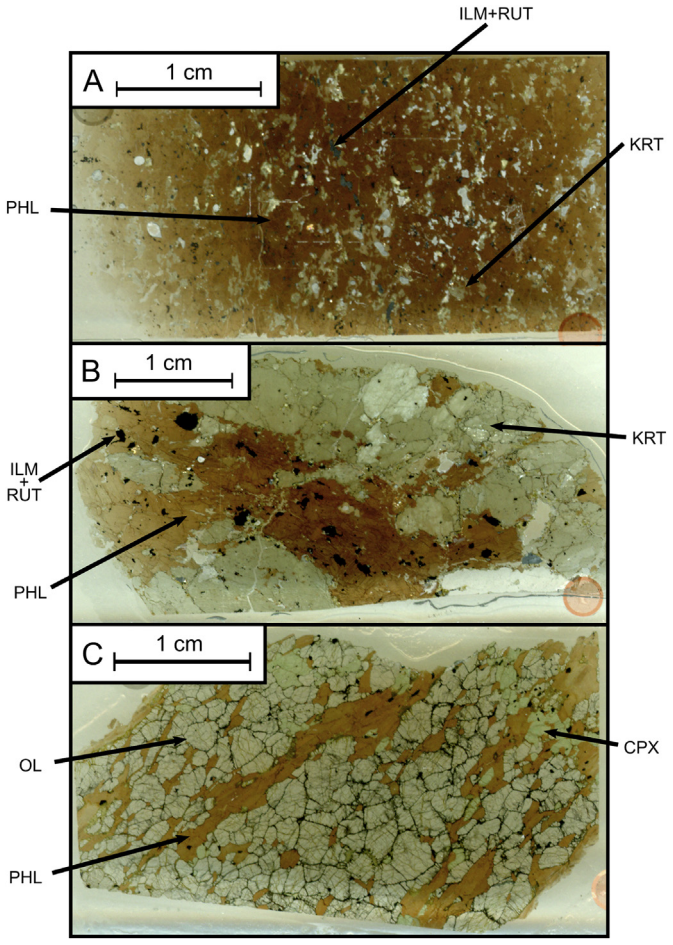

Fig. 2. Photomicrographs of MARID xenoliths. A: sample JJG-2326, displaying massive texture with homogeneous distribution of MARID phases (phl = phlogopite; krt = K-richterite; ilm = ilmenite; rut = rutile); B: sample AJE-2334, displaying distinct K-richterite- and phlogopite-rich layers; C: sample AJE-319, a dunite (ol = olivine) containing veins of phlogopite (phl) and clinopyroxene (cpx).

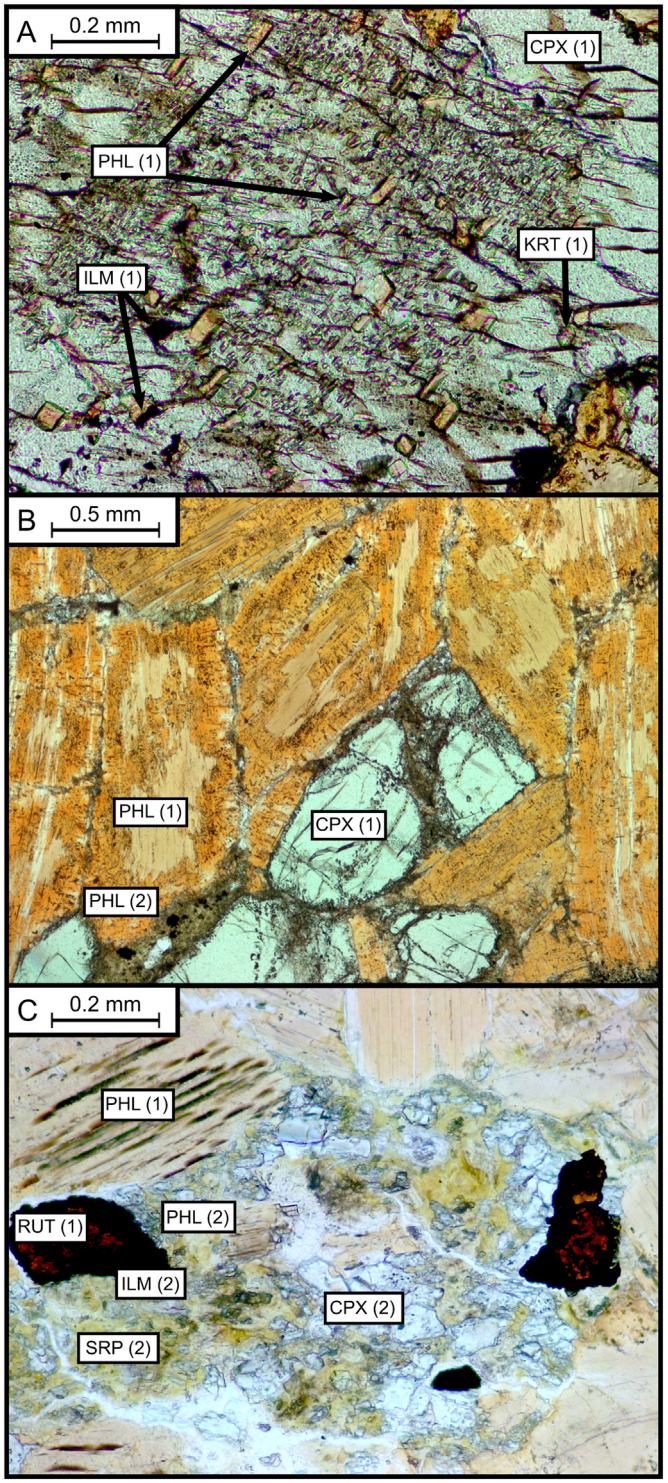

Fig. 3. Plane-polarised transmitted light photomicrographs. A: Clinopyroxene (cpx) in MARID sample AJE-333, containing abundant "primary" inclusions of phlogopite (phl), ilmenite (ilm), and K-richterite (krt). B: MARID sample WES-2, containing coarse-grained clinopyroxene and phlogopite. The phlogopite grains in this sample frequently display poikilitic overgrowths with different colours and textures to their cores; C: An example of a "secondary" vein in MARID sample KFDX-3, which is located between MARID phlogopite and rutile (rut) grains; the vein contains clinopyroxene, phlogopite and serpentine (srp, which is interpreted as secondary), and its formation appears to have resulted in black ilmenite overgrowths around primary rutile grains. The numbers proceeding mineral abbreviations indicate the inferred generation of each mineral, where (1) suggests "primary" MARID genesis, and (2) relates to "secondary" metasomatic events following the initial formation of MARID rocks.

Table 1
Modal mineral abundances (%) of main constituents of MARID and PIC xenoliths in this study, measured by point counting (≥2000 points per sample).

	Sample name	Locality	M	A	R	I	D	Accessory phases
MARID	AJE-2333	BLF	70 ± 14	22 ± 7	2 ± 1	2 ± 2	4 ± 4	ap, bar, cc, FeO, sulf
	AJE-2334	BLF	45 ± 6	51 ± 7	2 ± 1	2 ± 1	0	ap, bar, cc, ttn
	AJE-2335	BLF	43 ± 10	56 ± 9	1 ± 1	<1	0	ap, bar, cc, cel, FeO, sulf
	AJE-2422	BLF	86 ± 9	10 ± 6	2 ± 1	2 ± 2	0	ap, bar, cc, cel, FeO, ttn, sulf
	AJE-319[a]	DeB	80 ± 11	0	≪1	3 ± 3	17 ± 8	ap, cc, FeO, sp., sulf
	AJE-326	KIM	27 ± 3	67 ± 6	3 ± 2	3 ± 2	0	ap, bar, cc, pvk, sulf, ttn
	AJE-333	DeB	77 ± 2	0	2 ± 1	1 ± 1	20 ± 3	ap, cc, pvk, ttn
	AJE-335	DeB	82 ± 5	0	<1	<1	18 ± 5	ap, arm, bar, cc, sp., ttn
	AJE-360	BLF	96 ± 2	0	2 ± 1	2 ± 1	0	ap, bar, cc, FeO, pvk, ttn
	AJE-537	KAM	90 ± 2	0	<1	≪1	10 ± 3	cc, FeO, pvk, sulf, ttn
	AJE-559	KAM	~100	0	≪1	≪1	0	ap, bar, cc, ttn
	AJE-67	NEW	19 ± 9	65 ± 10	0	16 ± 4	0	ap, bar, cc, sulf
	AJE-69	NEW	18 ± 5	71 ± 7	0	11 ± 2	0	ap, bar, cc, sulf
	BLFX-26	BLF	43 ± 6	42 ± 5	2 ± 1	≪1	13 ± 3	bar, cc, FeO, pvk, sulf, ttn
	JJG-2040	BLF	79 ± 12	0	≪1	≪1	21 ± 12	ap, bar, cc, pvk, sulf, ttn
	JJG-2315	BLF	90 ± 4	5 ± 3	<1	≪1	4 ± 2	ap, arm, bar, cc, esk, FeO, sulf, ttn
	JJG-2326	BLF	91 ± 3	6 ± 2	2 ± 1	1 ± 1	0	ap, bar, cc, sulf, ttn
	JJG-2331	BLF	91 ± 4	4 ± 3	3 ± 2	2 ± 2	0	ap, arm, bar, cc, pvk, sp., sulf, ttn
	KFDX-3	KAM	99 ± 1	0	1 ± 1	≪1	0	bar, cc, sp., sulf, ttn
	KPX-1	KIM	~100	0	<1	<1	0	arm, cc, pvk, sp., ttn,
	WES-2	WES	75 ± 2	0	≪1	≪1	25 ± 2	ap, bar, cc, pvk, sulf, ttn
PIC	AJE-540	KAM	92 ± 3	0	0	2 ± 1	6 ± 3	ap, bar, cc, FeO, pvk, sp
	AJE-541	KAM	99 ± 1	0	0	≪1	1 ± 1	cc, esk, FeO, sp., ttn
	AJE-568	KAM	93 ± 3	0	0	1 ± 1	6 ± 3	ap, bar, cc, esk, FeO, pvk, ttn
	FW-20	BLF	80 ± 7	0	≪1	<1	20 ± 6	ap, cc, chr, esk, FeO, sp., sulf, ttn
	JJG-2327	BLF	93 ± 3	0	0	≪1	7 ± 3	cc, FeO, sp., pvk, ttn

BLF: Bultfontein; DeB: De Beers: KAM: Kamfersdam; KIM: Kimberley; NEW: Newlands; WES: Wesselton.
M: Mica (phlogopite); A: Amphibole (K-richterite); R: Rutile; I: Ilmenite; D: Diopside.
Accessory minerals – ap: apatite; arm: armalcolite; bar: barite; cc: carbonate (mostly calcite); cel: celestine; chr: chromatite ($CaCrO_4$); esk: eskolaite (Cr_2O_3); FeO: iron oxides (predominantly magnetite); pvk: perovskite; sp.: spinel (mostly Mg-ulvöspinel or magnesiochromite); sulf: sulfides (predominantly pentlandite); ttn: titanite.
Uncertainties are 2 s.d. based on analysis of multiple areas of each sample; only abundances of the main MARID-PIC minerals are reported.
[a] Modal abundances for sample AJE-319 refer only to veins, and not to the olivine-rich dunite portion of this sample.

clinopyroxene) into discrete bands (Fig. 2b). Such textures are common features of MARID rocks (Dawson and Smith, 1977; Waters, 1987a, 1987b). One sample (AJE-319) is a dunite that hosts discontinuous veins of phlogopite and clinopyroxene (Fig. 2c). Despite its olivine-rich composition, this sample was included in this investigation to determine (i) whether vein minerals display similar geochemistry to MARID-/PIC-suite minerals, and (ii) whether infiltration of the fluid/melt that produced the vein affected the dunite host. The grain sizes of the main MARID and PIC minerals in all of the studied xenoliths display a considerable range: phlogopite and K-richterite range from ~0.1 mm to 5 mm, clinopyroxene from ~0.1 mm to 3 mm, and rutile and ilmenite from <0.1 mm to 2 mm.

Modal mineral proportions were determined by point counting (≥2000 points) following examination of four areas of each sample. The complete mineral assemblages (i.e. phlogopite + K-richterite + diopside + ilmenite + rutile for MARID, and phlogopite + ilmenite + clinopyroxene for PIC) are rarely observed in individual xenoliths from this study, and mineral proportions are highly variable (Table 1). Phlogopite is the dominant phase in most of the studied samples (10 to ~100 vol%). K-richterite (0–75 vol%) is occasionally more abundant than phlogopite, but clinopyroxene (0–30 vol%) is never more abundant than phlogopite. Rutile and ilmenite are the least abundant of the MARID-PIC minerals (0–4 and 0–20 vol%, respectively). The variability described in the samples from this study is typical for MARID and PIC rocks (e.g., Dawson and Smith, 1977), and serves to illustrate why they should not be classified based on modal mineral proportions alone (Grégoire et al., 2002). Mineral major element compositions are a more effective, quantitative classification tool for these phlogopite-rich rocks.

In the MARID samples examined here, mineral grains frequently contain what are apparently primary inclusions of the main coexisting MARID phases (e.g., phlogopite inclusions in clinopyroxene; Fig. 3a), suggesting that the different MARID minerals formed concurrently, during the same event. Some MARID samples contain minerals that display chemical zonation, which is particularly notable in the differing colours and textures of phlogopite cores and overgrowths (Fig. 3b). The overgrowths probably formed after the main MARID genesis event, perhaps coeval with kimberlite magmatism (e.g., Giuliani et al., 2016, and references therein). A variety of accessory minerals including clinopyroxene, phlogopite, titanite, carbonates (calcite, with minor strontianite), barite, celestine, sulfides (commonly pentlandite), apatite, perovskite, Cr-spinel, armalcolite, eskolaite (Cr_2O_3), chromatite ($CaCrO_4$), and magnetite, were observed in the MARID rocks from this study (Table 1). These accessory minerals occur along mineral cleavages and grain boundaries, and are included in zoned rims (notably of clinopyroxene) and/or in serpentine-carbonate veins, and are much finer-grained than the main MARID minerals (Fig. 3c; <80 μm, compared to >200 μm; Fitzpayne et al., 2018). Although zircons have been observed in previous studies of MARID rocks (e.g., Giuliani et al., 2015; Konzett et al., 2000) and were interpreted as primary constituents of the MARID assemblage, no zircon was found in any of the samples examined in this study. The distribution of the accessory minerals described herein suggests that these minerals formed after the main MARID genesis event (e.g., Dawson and Smith, 1977; Fitzpayne et al., 2018).

Clinopyroxene grains in PIC xenoliths occasionally include PIC phlogopite and ilmenite. The main PIC phases are >200 μm in length. Although serpentine-carbonate veins were not observed in the PIC samples examined in this study, rare "pools" of serpentine containing fine-grained (<50 μm) oxide minerals (predominantly magnetite, rutile, ilmenite, and Cr-spinel) occur in all but two PIC samples (AJE540; AJE541). One PIC sample (FW-20) also contains accessory rutile intergrown with ilmenite. Fine-grained (<100 μm) calcite commonly occurs along grain boundaries in PIC samples, and appears to postdate the main PIC genetic event (see Fitzpayne et al., 2018).

Table 2
MARID and PIC mineral major element averages (± 1 s.d.) measured by EPMA in this study, compared to previous data.

	Phlogopite					K-richterite			Clinopyroxene
	MARID: This study (n = 210)	PIC: This study (n = 42)	Literature MARID (n = 57)	Literature peridotite (n = 68)	Literature glimmerite (n = 25)	MARID: This study (n = 122)	Literature MARID (n = 34)	Literature peridotite (n = 8)	MARID: This study (n = 107)
SiO_2	42.54 ± 0.91	41.23 ± 0.54	42.15 ± 0.81	41.19 ± 1.53	40.59 ± 1.07	54.62 ± 0.80	54.69 ± 0.97	54.26 ± 1.27	54.71 ± 0.62
TiO_2	1.48 ± 0.88	1.35 ± 0.44	1.23 ± 0.82	1.45 ± 1.22	1.07 ± 0.72	0.52 ± 0.17	0.57 ± 0.23	0.59 ± 0.25	0.11 ± 0.04
Al_2O_3	9.91 ± 0.68	11.95 ± 0.51	9.86 ± 0.87	12.23 ± 1.27	12.68 ± 0.84	1.04 ± 0.27	1.07 ± 0.42	1.31 ± 0.30	0.42 ± 0.22
Cr_2O_3	0.18 ± 0.11	0.29 ± 0.20	0.19 ± 0.16	0.83 ± 0.57	0.75 ± 0.65	0.21 ± 0.14	0.20 ± 0.12	0.38 ± 0.23	0.78 ± 0.55
FeO^T	6.78 ± 1.05	3.90 ± 0.18	6.94 ± 1.73	3.72 ± 0.85	4.54 ± 2.06	3.92 ± 0.91	3.99 ± 1.00	2.74 ± 0.52	4.58 ± 0.85
MnO	0.04 ± 0.02	0.03 ± 0.01	0.04 ± 0.02	0.03 ± 0.02	0.16 ± 0.16	0.05 ± 0.02	0.05 ± 0.02	0.04 ± 0.02	0.13 ± 0.04
MgO	23.68 ± 1.42	25.04 ± 0.49	23.99 ± 1.41	24.95 ± 1.46	24.34 ± 2.31	21.31 ± 0.75	21.38 ± 0.88	22.41 ± 0.34	15.92 ± 0.72
ZnO	0.08 ± 0.10	0.06 ± 0.03	n/a	n/a	n/a	n/a	n/a	n/a	n/a
NiO	0.12 ± 0.05	0.12 ± 0.04	0.11 ± 0.05	0.18 ± 0.05	0.12 ± 0.09	n/a	n/a	n/a	n/a
CaO	0.05 ± 0.08	0.05 ± 0.04	0.08 ± 0.14	0.03 ± 0.02	0.03 ± 0.04	6.82 ± 0.39	6.74 ± 0.52	7.07 ± 0.25	21.83 ± 0.98
Na_2O	0.13 ± 0.06	0.18 ± 0.05	0.15 ± 0.09	0.30 ± 0.18	0.21 ± 0.17	3.52 ± 0.46	3.56 ± 0.47	3.28 ± 0.48	1.31 ± 0.46
K_2O	10.11 ± 0.36	10.53 ± 0.23	10.16 ± 0.48	10.12 ± 0.59	10.22 ± 0.53	5.09 ± 0.45	4.98 ± 0.42	5.17 ± 0.54	0.07 ± 0.12
F	0.33 ± 0.15	0.34 ± 0.14	0.42 ± 0.17	0.28 ± 0.23	0.71 ± 0.33	0.29 ± 0.14	0.44 ± 0.15	n/a	n/a
Cl	0.04 ± 0.02	0.03 ± 0.01	0.03 ± 0.02	0.05 ± 0.02	0.04 ± 0.02	0.02 ± 0.01	0.02 ± 0.01	n/a	n/a
	Clinopyroxene			Rutile		Ilmenite			
	PIC: This study (n = 55)	Literature MARID (n = 26)	Literature peridotite (n = 270)	MARID: This study (n = 81)	Literature MARID (n = 9)	MARID: This study (n = 95)	PIC: This study (n = 17)	Literature MARID (n = 14)	Literature peridotite (n = 3)
SiO_2	54.35 ± 0.84	54.53 ± 0.64	54.45 ± 1.23	n/a	n/a	0.03 ± 0.06	0.03 ± 0.01	0.04 ± 0.13	n/a
TiO_2	0.35 ± 0.05	0.27 ± 0.17	0.24 ± 0.32	95.41 ± 2.80	95.87 ± 2.56	52.30 ± 2.35	55.72 ± 1.28	53.38 ± 1.23	55.78 ± 2.95
Al_2O_3	1.89 ± 0.26	0.49 ± 0.20	2.59 ± 1.46	n/a	n/a	0.04 ± 0.02	0.27 ± 0.09	0.06 ± 0.08	0.18 ± 0.13
Cr_2O_3	1.07 ± 0.15	0.52 ± 0.25	1.71 ± 0.90	1.79 ± 1.14	1.39 ± 0.87	1.23 ± 1.11	1.57 ± 0.36	1.21 ± 0.37	1.71 ± 0.28
FeO^T	3.17 ± 0.14	4.97 ± 0.77	2.73 ± 1.32	1.01 ± 1.28	1.31 ± 1.76	35.14 ± 3.70	25.83 ± 2.18	35.28 ± 1.97	25.14 ± 7.77
V_2O_3	n/a	n/a	n/a	0.50 ± 0.13	n/a	0.31 ± 0.06	0.29 ± 0.05	n/a	n/a
MnO	0.08 ± 0.02	0.14 ± 0.03	0.09 ± 0.04	n/a	n/a	0.41 ± 0.11	0.30 ± 0.05	0.42 ± 0.06	0.28 ± 0.03
MgO	16.70 ± 0.34	17.05 ± 1.04	16.62 ± 1.63	0.17 ± 0.24	0.20 ± 0.22	9.48 ± 1.86	15.16 ± 1.46	9.69 ± 1.20	16.55 ± 5.08
ZnO	n/a	n/a	n/a	0.10 ± 0.12	n/a	0.08 ± 0.10	0.05 ± 0.03	n/a	n/a
NiO	n/a	n/a	n/a	n/a	n/a	0.11 ± 0.06	0.15 ± 0.05	0.10 ± 0.06	0.10 ± 0.10
CaO	20.06 ± 0.43	20.67 ± 1.03	19.41 ± 2.24	0.19 ± 0.17	0.04 ± 0.04	0.05 ± 0.03	0.09 ± 0.08	0.07 ± 0.06	0.04 ± 0.01
Na_2O	1.87 ± 0.20	1.23 ± 0.28	2.05 ± 1.28	n/a	n/a	n/a	n/a	n/a	n/a
K_2O	0.11 ± 0.21	0.04 ± 0.02	0.02 ± 0.10	n/a	n/a	n/a	n/a	n/a	n/a
Nb_2O_5	n/a	n/a	n/a	0.93 ± 1.07	n/a	0.14 ± 0.15	0.10 ± 0.03	0.33 ± 0.01	0.13 ± 0.23

5. Mineral chemistry

To obtain representative major and trace element compositions of minerals from each sample, five to ten grains of each MARID or PIC mineral were analysed in thin section. Mineral compositions are generally homogeneous within a single sample, and the ranges of values are due to variations between samples. All chemical analyses acquired in this study are presented in Appendix A. Considerably larger compositional variability is associated with rims of MARID phases that are in contact with late-stage serpentine-carbonate veins, and vein minerals. These compositions have been omitted from this study because the development of these rims and vein minerals are likely linked to kimberlite infiltration that occurred shortly before or during xenolith entrainment by kimberlite magmas (Fitzpayne et al., 2018).

5.1. Major element compositions

The only previous comparative study between MARID and PIC rocks (Grégoire et al., 2002) proposed the following criteria to distinguish these rocks, which have been applied to the samples in this study:

1. higher Al_2O_3 and Mg# in PIC phlogopite;
2. higher MgO and TiO_2 in PIC ilmenite;
3. differences in clinopyroxene trace element patterns, most notably negative and positive Zr-Hf anomalies in MARID and PIC clinopyroxene, respectively.

The sample set can thus be divided into 21 MARID and 5 PIC samples. The major element compositions acquired in this study are summarised in Table 2 along with compositional variations of MARID and peridotite minerals from previous studies.

5.1.1. Phlogopite

Phlogopite in MARID samples contains between 8.1 and 12.0 wt% Al_2O_3, whereas phlogopite from PIC samples is slightly more Al-rich (10.7–12.6 wt% Al_2O_3). MARID and PIC phlogopite are both deficient in [Si + Al] (7.6–8.0 apfu and 7.8–8.0 apfu, respectively), as noted in previous studies (e.g., Dawson and Smith, 1977). This deficiency appears to be compensated by Fe^{3+} and Ti^{4+} substitution into the tetrahedral site. MARID and PIC phlogopite contain similar TiO_2 contents (1.5 ± 0.9 wt%, n = 201; and 1.4 ± 0.4 wt%, n = 42, respectively, 1 s.d.), but MARID phlogopite has a lower Mg# (100 * Mg/(Mg + Fe)) than PIC phlogopite (79.2–89.7 and 89.7–92.6, respectively). Phlogopite derived from veins in dunite sample AJE-319 falls within both peridotite and MARID phlogopite fields (10.0 ± 0.2 wt% Al_2O_3; 0.6 ± 0.1 wt% TiO_2; Mg# = 89.5 ± 0.3; n = 9, 1 s.d.; Fig. 4).

Fig. 4 shows that the major element compositions of MARID phlogopite analysed in this study mostly fall within the ranges of previously published MARID data. As noted by Grégoire et al. (2002), PIC phlogopite compositions are unlike MARID, and plot entirely within the broad compositional range for peridotitic phlogopite, although the two ranges do have significant overlap in terms of TiO_2, Al_2O_3, Cr_2O_3 and Na_2O contents.

5.1.2. Potassic richterite

Amphibole in MARID xenoliths is classified as potassic (or K-) richterite, due to its high K_2O (5.1 ± 0.5 wt%; 1 s.d., n = 122) and Na_2O (3.5 ± 0.5 wt%) contents, relative to CaO (6.8 ± 0.4 wt%) and Al_2O_3 (1.0 ± 0.3 wt%). In this study, the average FeO^T and Cr_2O_3 contents of MARID K-richterite are 3.9 ± 0.9 wt% and 0.21 ± 0.14 wt%, respectively. K-richterite in peridotite xenoliths generally displays higher Cr and lower Fe contents than MARID K-richterite, although some overlap can also be seen (Table 2; Fig. 5a).

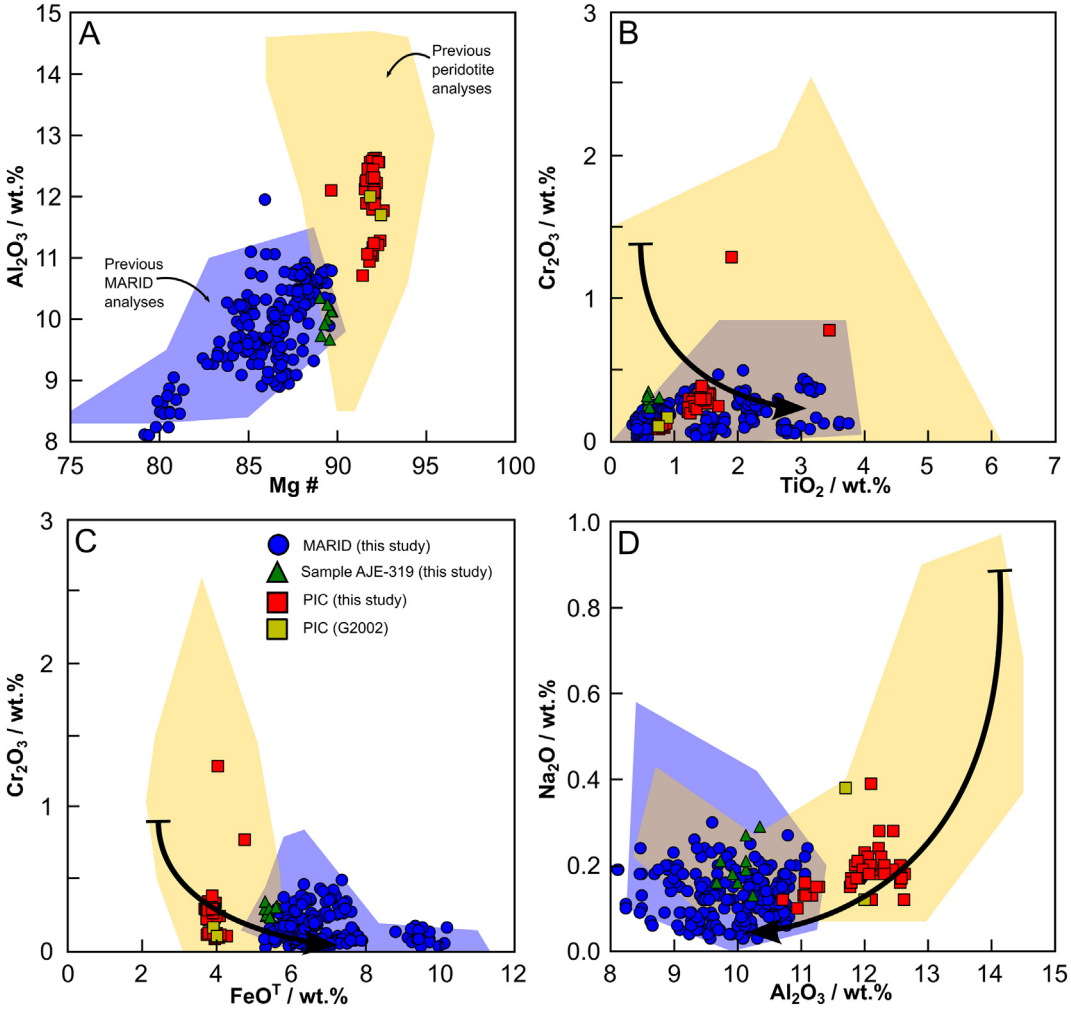

Fig. 4. A: wt% Al_2O_3 vs Mg# (100*Mg/(Mg + Fe)); B: wt% Cr_2O_3 vs wt% TiO_2; C: wt% Cr_2O_3 vs wt% FeO^T; and D: wt% Na_2O vs wt% Al_2O_3 in phlogopite from MARID and PIC samples analysed in this study. Yellow squares represent analyses of PIC phlogopite in G2002 (Grégoire et al., 2002). Blue and orange fields represent compositional ranges for southern African MARID (Banerjee et al., 2015; Boyd, 1990; Dawson and Smith, 1977; Erlank et al., 1987; Giuliani et al., 2013, 2016; Grégoire et al., 2002; Jones et al., 1982; Konzett et al., 2000, 2014; Matson et al., 1986; Sweeney et al., 1993; Waters et al., 1989) and peridotitic phlogopite, respectively (Boyd, 1990; Dawson and Smith, 1977, and references therein; Erlank et al., 1987, and references therein; Giuliani et al., 2016; Grégoire et al., 2002; Jones et al., 1982; Konzett et al., 2000, 2013; le Roex and Class, 2016; Matson et al., 1986; Rehfeldt et al., 2007, 2008; Stiefenhofer et al., 1997, and references therein; Waters et al., 1989; Winterburn et al., 1990). Black arrows show the change in mineral composition with progressive metasomatism as described by Erlank et al. (1987) for the GP to PKP sequence.

5.1.3. Clinopyroxene

MARID clinopyroxene is typically diopside (Ca# = 100 * Ca/(Ca + Mg) = 48.3–51.3) with variable Mg# (81.7–91.5). In comparison, PIC clinopyroxene is more subcalcic (Ca# = 44.6–47.5), with generally higher Mg# (89.0–91.0). MARID clinopyroxene contains low abundances of TiO_2, Al_2O_3 and Na_2O (0.11 ± 0.04 wt%, 0.42 ± 0.22 wt%, 1.3 ± 0.5 wt%, respectively; 1 s.d., n = 97) compared to PIC clinopyroxene (0.4 ± 0.1 wt% TiO_2, 1.9 ± 0.3 wt% Al_2O_3, 1.9 ± 0.2 wt% Na_2O; n = 55; Fig. 5b–d). Clinopyroxene in veins in dunite sample AJE-319 is compositionally identical to MARID clinopyroxene (0.08 ± 0.01 wt% TiO_2; 0.13 ± 0.01 wt% Al_2O_3; 1.0 ± 0.1 wt% Na_2O; Mg# = 90.9 ± 0.2, Ca# = 48.8 ± 0.3; n = 10, 1 s.d.).

The Cr_2O_3-TiO_2 systematics of many MARID clinopyroxene data from this study are significantly different to previously published analyses (Erlank et al., 1987), extending to much higher Cr_2O_3 and occurring within a very limited range of TiO_2 contents (Fig. 5b). This is probably because the range of MARID clinopyroxene compositions compiled by Erlank et al. (1987; Fig. 5b) includes analyses of secondary Ti-rich clinopyroxene, with an origin likely unrelated to MARID genesis (e.g., Dawson and Smith, 1977; Fitzpayne et al., 2018). On the other hand, MARID clinopyroxene FeO^T-Al_2O_3 systematics in this study are consistent with previous analyses (Fig. 5c).

5.1.4. Ilmenite

Ilmenite in MARID samples has higher FeO^T (35 ± 4 wt%), and lower TiO_2 (52 ± 2 wt%) and MgO (9 ± 2 wt%; 1 s.d.; n = 87) contents than ilmenite in PIC samples (26 ± 2 wt% FeO^T; 56 ± 1 wt% TiO_2; 15 ± 1 wt% MgO; 1 s.d.; n = 17). Ilmenite in veins in sample AJE-319 closely resembles MARID ilmenite (32 ± 1 wt% FeO^T; 50 ± 1 wt% TiO_2; 11 ± 1 wt% MgO; n = 8). Fig. 6 shows that MARID ilmenite analyses from this study slightly extend the range of MgO-TiO_2 compositions compared to previous MARID results, whereas PIC ilmenite closely matches the composition of ilmenite in metasomatised peridotites.

5.1.5. Rutile

Rutile in MARID xenoliths from this study shows broad inter-sample compositional variations, particularly in terms of the concentrations of FeO^T (0.0–5.6 wt%), Cr_2O_3 (0.4–4.4 wt%), and Nb_2O_5 (0.0–5.2 wt%). Previous analyses of rutile in MARID rocks also show wide ranges of FeO^T (0.0–5.5 wt%) and Cr_2O_3 (0.5–4.7 wt%) contents (Banerjee et al., 2018; Boyd, 1990; Dawson and Smith, 1977; Grégoire et al., 2002; Waters, 1987a, 1987b); Nb_2O_5 was only analysed by Waters (1987b), and was also highly variable (0.3–10.7 wt%).

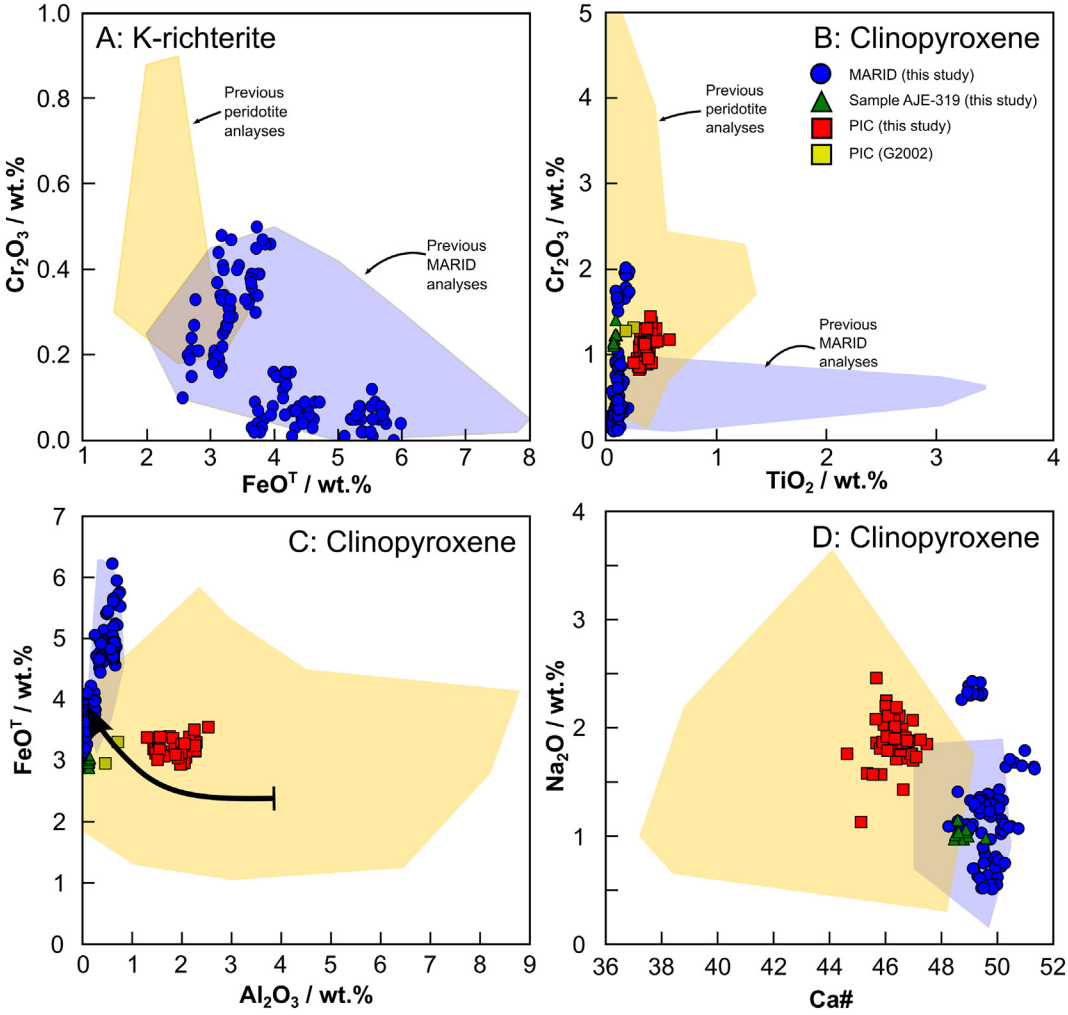

Fig. 5. A: wt% Cr_2O_3 vs wt% FeO^T in K-richterite from MARID samples in this study; B: wt% Cr_2O_3 vs wt% TiO_2; C: wt% FeO^T vs wt% Al_2O_3; and D: wt% Na_2O vs Ca# (100*Ca/(Ca + Mg)) in clinopyroxene from MARID and PIC samples from this study. Blue and orange fields indicate the compositional ranges of southern African MARID (Boyd, 1990; Dawson and Smith, 1977, and references therein; Erlank et al., 1987, and references therein; Giuliani et al., 2013; Grégoire et al., 2002; Jones et al., 1982; Konzett et al., 2000, 2013, 2014; Sweeney et al., 1993; Waters et al., 1989) and peridotitic minerals, respectively (Boyd, 1990; Carswell et al., 1979; Dawson and Smith, 1977, and references therein; Erlank et al., 1987, and references therein; Grégoire et al., 2002, 2003, 2005; Hin et al., 2009; Jones et al., 1982; Katayama et al., 2009; Konzett et al., 2000; Lazarov et al., 2009; le Roex and Class, 2016; MacGregor, 1979; Rehfeldt et al., 2008; Simon et al., 2003; Stiefenhofer et al., 1997; van der Meer et al., 2013; Viljoen et al., 2009; Wasch et al., 2009; Waters et al., 1989; Winterburn et al., 1990).

5.1.6. Olivine

Olivine occurs in only one of the studied samples (AJE-319), as part of the dunitic host to the clinopyroxene-phlogopite-rich veins. Olivine cores have relatively Fe-rich compositions (Mg# = 88.0 ± 0.1; 40.2 ± 0.1 wt% SiO_2; 0.37 ± 0.03 wt% NiO; n = 6, 1 s.d.) compared to other peridotitic olivine from xenoliths derived from the Kimberley kimberlites (typically Mg# from 88 to 93; Erlank et al., 1987). There is no evidence of compositional zonation in the olivine in sample AJE-319, and no variations in grains that are in contact with the phlogopite-rich veins.

5.2. Trace element compositions

5.2.1. Phlogopite

Phlogopite in PIC and MARID xenoliths, and in the AJE-319 veins, displays positive anomalies in Pb, Sr, and HFSE on primitive mantle-normalised trace element diagrams (Fig. 7a), and contains very low abundances of REE. Compared to MARID phlogopite, PIC phlogopite is typically depleted in Th and U and slightly enriched in HFSE (Fig. 7a). MARID phlogopite compositions vary significantly between samples (e.g., Nb/U = from <1 to 210). By contrast, PIC phlogopite has a consistently higher Nb/U ratio (>230; Fig. 7a). MARID and PIC phlogopite trace element compositions are broadly similar to the compositions of phlogopite from peridotite and pyroxenite xenoliths from Kimberley (Giuliani et al., 2016; Rehfeldt et al., 2008; Fig. 7a).

5.2.2. Potassic richterite

Primitive mantle-normalised trace element patterns of K-richterite in MARID rocks are enriched in light rare earth elements (LREE; chondrite-normalised La/Yb > 12). Trace element patterns exhibit characteristic positive anomalies for Pb, Sr, Hf and Ti, resembling previously published analyses of MARID K-richterite (Fig. 7b). The few published trace element analyses of K-richterite from metasomatised PKP rocks from southern African localities (Grégoire et al., 2002; Konzett et al., 2000) have similar primitive mantle-normalised patterns to K-richterite in MARID xenoliths from this study (Fig. 7b).

5.2.3. Clinopyroxene

Primitive mantle-normalised trace element patterns of MARID clinopyroxene from this study exhibit pronounced negative anomalies in Pb, Zr-Hf, and Ti (Fig. 8a). The trace element patterns of clinopyroxene in the veins of sample AJE-319 are indistinguishable from those of MARID clinopyroxene (Figs. 8a, 9a). Clinopyroxene in MARID xenoliths is enriched in LREE (La = 20.5 ± 9.8 ppm; Ce: 72.7 ± 32.5 ppm; 1 s.d., n = 69).

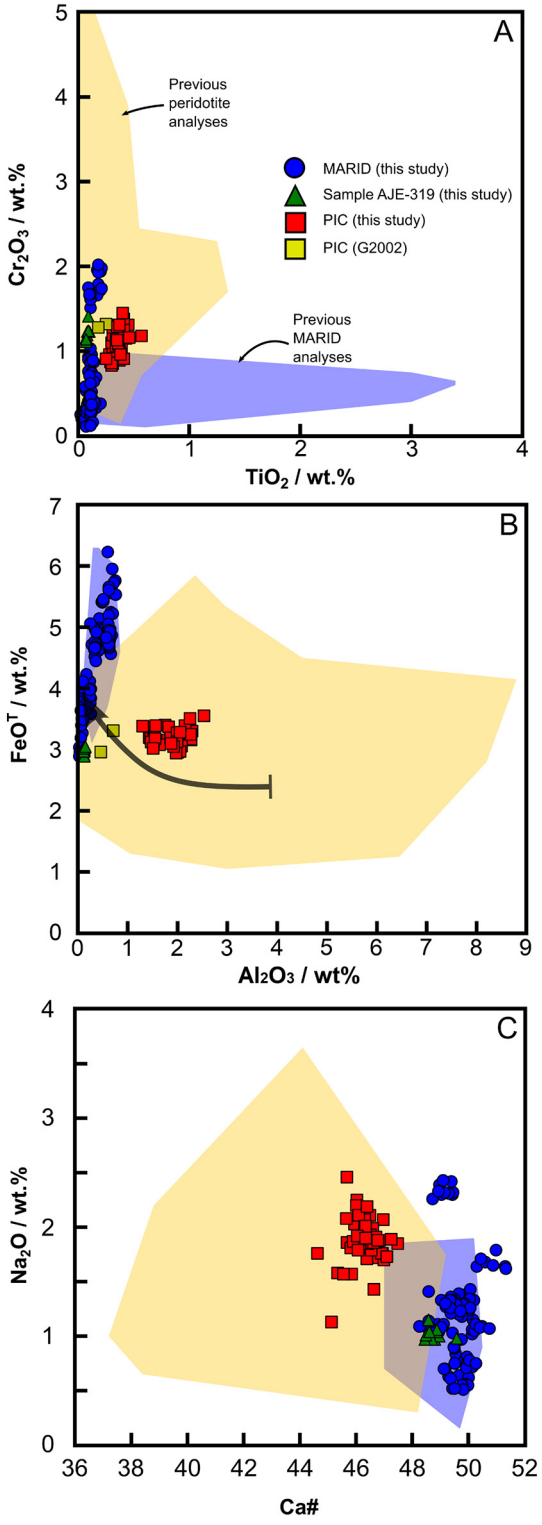

Fig. 6. wt% MgO vs wt% TiO_2 in ilmenite in MARID and PIC samples from this study; symbols as in Fig. 4. Blue and orange fields indicate the compositional ranges of southern African MARID (Dawson and Smith, 1977; Erlank et al., 1987; Grégoire et al., 2002; Konzett et al., 2014) and peridotite ilmenite, respectively (Grégoire et al., 2002; Konzett et al., 2000).

Clinopyroxene in PIC xenoliths can be distinguished from MARID clinopyroxene by the absence of negative Zr-Hf anomalies (Fig. 8b; Appendix A), and significantly lower REE concentrations (La = 2.5 ± 0.7 ppm; Ce = 10.2 ± 1.8 ppm; n = 33; Fig. 9a) and chondrite-normalised

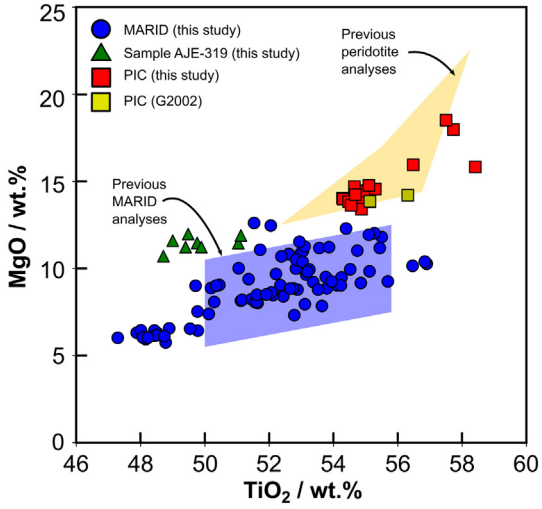

Fig. 7. Primitive mantle-normalised trace element diagrams; normalising values from McDonough and Sun (1995). A: Average and range of MARID and PIC phlogopite compositions from this study, compared to phlogopite compositions from R2008 (Rehfeldt et al., 2008) and G2016 (Giuliani et al., 2016; this also includes data for lherzolites, wehrlites, harzburgites in Giuliani et al., 2013, 2014, and Grégoire et al., 2002); B: Average and range of MARID K-richterite compositions from this study, compared to MARID K-richterite from G2002 (Grégoire et al., 2002) and G2013 (Giuliani et al., 2013), and peridotite K-richterite from K2000 (Konzett et al., 2000) and G2002.

LREE/HREE ratios (Ce/Yb_N: MARID = 16–60, PIC = 11–21; Fig. 8c). The new MARID and PIC clinopyroxene trace element data reported here resemble those collected by Grégoire et al. (2002), except for the

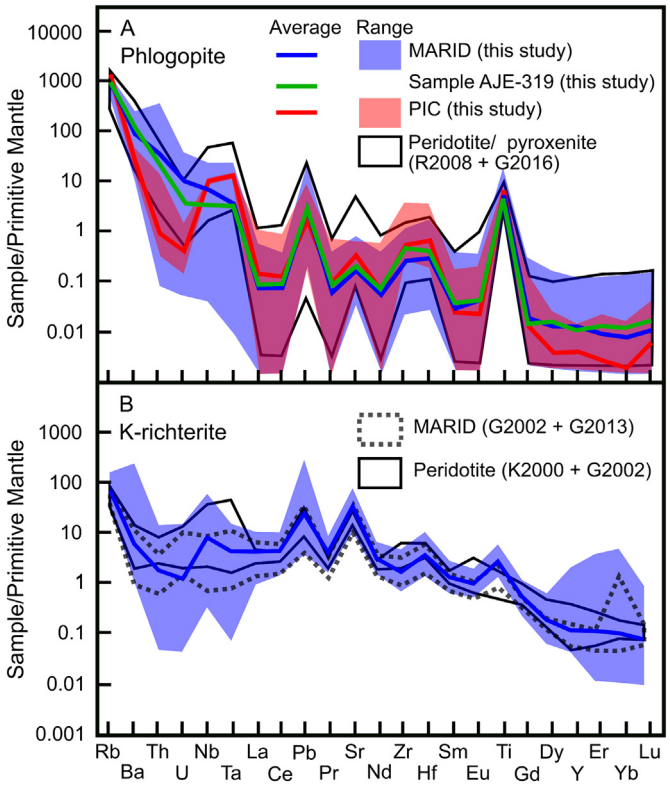

Fig. 8. Primitive mantle-normalised trace element (panels A and B) and chondrite-normalised REE (panel C) diagrams for clinopyroxene in MARID-PIC samples from this study. All normalising values from McDonough and Sun (1995). A: Average and range for MARID clinopyroxene and clinopyroxene in veins from sample AJE-319 in this study, compared to data from G2002 (Grégoire et al., 2002); B: Average and range for PIC clinopyroxene in this study, compared to data from G2002; C: Averages and ranges of REE contents in MARID-PIC clinopyroxene and clinopyroxene in sample AJE-319 in this study; symbols as in A and B.

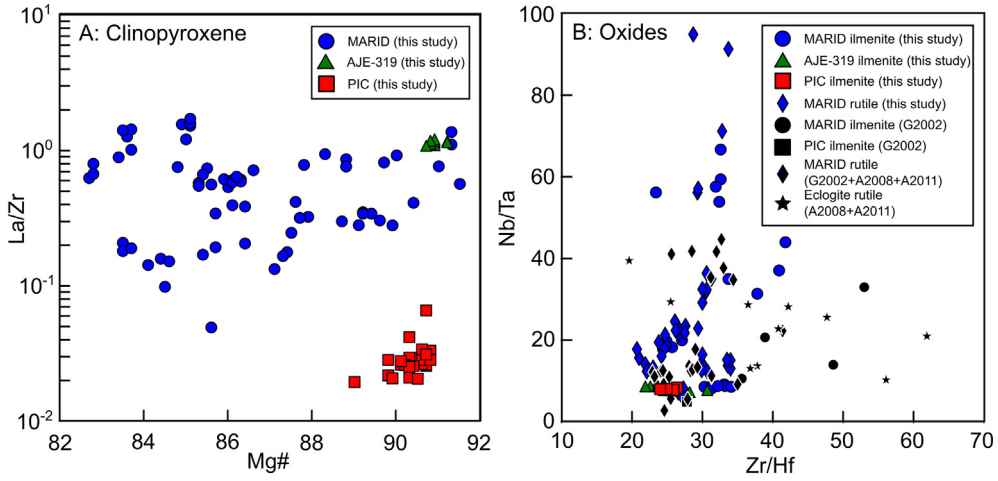

Fig. 9. (A) La/Zr vs Mg# in clinopyroxene from MARID (blue circles), veins in sample AJE-319 (green triangles) and PIC (red squares) samples from this study; note log scale on y-axis; (B) Nb/Ta vs Zr/Hf ratios in ilmenite from MARID and PIC samples, rutile from MARID, and ilmenite from veins in sample AJE-319 (all data obtained in this study), compared to literature data for ilmenite and rutile in MARID, PIC and eclogite xenoliths (Aulbach et al., 2008, 2011; Grégoire et al., 2002).

difference in Pb anomalies in PIC clinopyroxene (absent or slightly positive versus typically negative in this study; Fig. 8b).

5.2.4. Ilmenite

MARID ilmenite generally contains lower abundances of HFSE than PIC ilmenite (e.g., Zr: 210 ± 130 ppm vs 470 ± 60 ppm; Ta: 51 ± 39 ppm vs 86 ± 5 ppm). MARID ilmenite exhibits wide ranges in Nb/Ta (22.8 ± 19.1) and Zr/Hf (30.0 ± 4.5), which overlap with PIC ilmenite Nb/Ta (8.0 ± 0.3) and Zr/Hf (28.1 ± 2.8; MARID n = 55, PIC n = 13; 1 s.d.; Fig. 9b). These mean values fall within the ranges reported by Grégoire et al. (2002; Fig. 9b). Ilmenite in veins in sample AJE-319 is compositionally identical to MARID ilmenite (Zr: 230 ± 30 ppm; Ta: 42 ± 5 ppm; Nb/Ta: 8.5 ± 0.6; Zr/Hf: 24.1 ± 3.1; n = 8).

5.2.5. Rutile

It was not possible to analyse the trace element composition of rutile from the only rutile-bearing PIC sample (FW-20), due to its occurrence as fine-grained (<30 μm) intergrowths with ilmenite. MARID rutile Nb/Ta ratios collected in this study vary significantly (43.9 ± 20.9; 1 s.d., n = 59), similar to the variability in MARID ilmenite (Fig. 9b). Rutile Zr/Hf (28.2 ± 3.5) also resembles that of MARID ilmenite. Previous analyses of MARID rutile (Aulbach et al., 2011; Grégoire et al., 2002) yielded similar variations in Nb/Ta (5–41) and Zr/Hf (24–42). Eclogitic rutile also exhibits wide ranges in both Nb/Ta (10–40) and Zr/Hf (20–62; Aulbach et al., 2008, 2011; Fig. 9b).

6. Bulk-rock reconstructions

Bulk-rock compositions of MARID and PIC samples have been reported in several studies (e.g., Grégoire et al., 2002; Waters, 1987a, 1987b). However, XRF-based and solution-mode determinations of bulk-rock compositions fail to account for the ubiquitous late-stage modification of mantle samples, including MARID rocks, entrained by kimberlites (e.g., carbonate veins, mineral zonation; cf. Dawson and Smith, 1977; Fitzpayne et al., 2018; Richardson et al., 1985; Simon et al., 2007). Calculation of reconstructed bulk-rock compositions therefore appears to be the most accurate method of determining the bulk composition of mantle samples such as MARID and PIC rocks prior to kimberlite entrainment. To perform bulk-rock reconstructions, the modal abundance of each primary MARID-PIC phase (determined by point-counting; Table 1) was combined with average mineral major and trace element compositions (Appendix A). Mineral proportions were converted to weight percentage abundances using the following densities: phlogopite = 2.79 g/cm^3; K-richterite = 3.10 g/cm^3; rutile = 4.25 g/cm^3; ilmenite = 4.79 g/cm^3; clinopyroxene = 3.28 g/cm^3 (data from www.mindat.org; last accessed on 16/04/2018).

The samples under investigation are extremely heterogeneous, and the mineral abundance ranges presented in Table 1 may not be entirely representative of each sample. Monte Carlo simulations were therefore performed in order to assess the uncertainties associated with (i) mineral abundance estimates; (ii) ranges in mineral composition collected in each sample; and (iii) mineral densities used, which are only representative of idealised end-member compositions. The methods by which Monte Carlo simulations were performed are presented in Appendix B. Based on the Monte Carlo simulations, the average (i.e. most likely) bulk-rock compositions of all samples from this study are presented in Appendix C.

The reconstructed whole-rock major element compositions of MARID samples are mafic-ultramafic (39–49 wt% SiO_2) and ultrapotassic (5.0–10.1 wt% K_2O; $K_2O/Na_2O > 2.5$), whereas PIC rocks are ultramafic and ultrapotassic (40–44 wt% SiO_2; 8.1–10.4 wt% K_2O; $K_2O/Na_2O > 21$). Reconstructed bulk-MARID compositions contain high and variable FeO^T contents (7.1 ± 2.3 wt%; Mg# = 84.6 ± 5.2; 1 s.d., n = 21), and are depleted in Al_2O_3 (7.1 ± 2.3 wt%) relative to reconstructed bulk-PIC compositions (FeO^T = 4.1 ± 0.3 wt%; Mg# = 91.3 ± 0.6; Al_2O_3 = 10.8 ± 1.4 wt%; 1 s.d., n = 5). Bulk-MARID and -PIC reconstructed major element compositions are broadly similar to previous bulk-rock analyses of these samples (Supplementary Table 1; Grégoire et al., 2002; Waters, 1987a). However, relative differences of up to 70% can be found between MARID bulk-rock reconstructions (Appendix C; this study) and bulk-rock analyses (Supplementary Table 1; Waters, 1987a) performed on the same samples, particularly in SiO_2, FeO^T, CaO and P_2O_5.

Calculated bulk-MARID and -PIC reconstructions exhibit a range of trace element compositions (Fig. 10) that are mainly controlled by their modal mineral proportions. The average reconstructed bulk-PIC composition is depleted in most of the incompatible trace elements (e.g., Th-U-P-LREE) compared to previous bulk-rock analyses by Grégoire et al. (2002; Fig. 10a). Part of this depletion is attributed to the clinopyroxene-rich nature of the PIC samples analysed by Grégoire et al. (2002; 36.8 vol.% vs ~8 vol.% in this study). A second bulk-rock reconstruction was performed for PIC samples using the average mineral compositions in this study (Appendix A) and the average mineral modal abundances of the two PIC samples of Grégoire et al. (2002; 61.6% phlogopite + 1.55% ilmenite + 36.85% clinopyroxene; "Average bulk-PIC**" in Fig. 10a; Appendix C). This

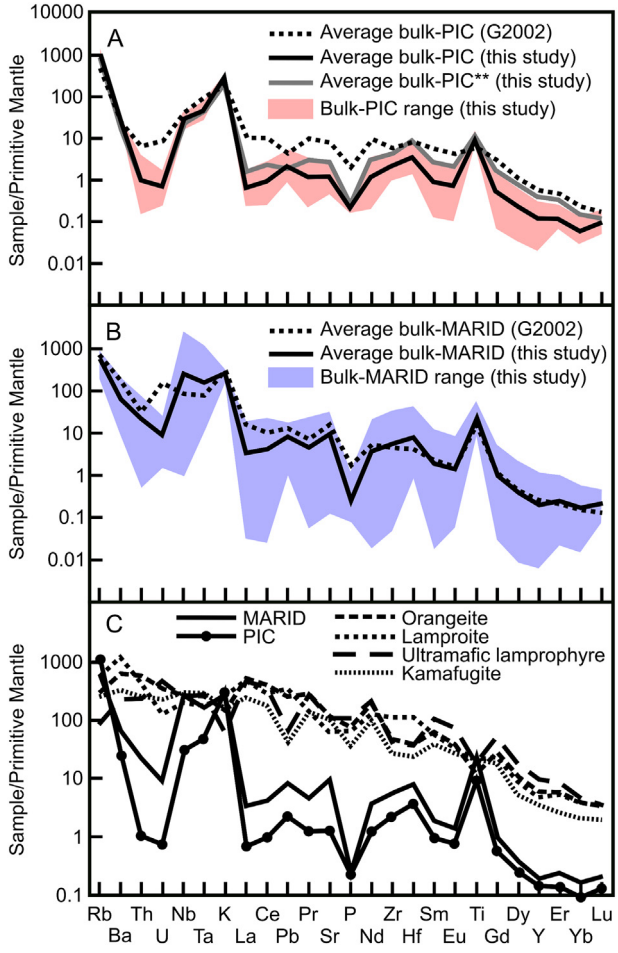

Fig. 10. Primitive mantle-normalised trace element diagrams plotting the range of bulk-PIC (A) and –MARID (B) reconstructions from this study, compared to MARID-PIC bulk-rock analyses in G2002 (Grégoire et al., 2002); normalising values from McDonough and Sun (1995). Solid grey line (average bulk-PIC**) in (A) is a bulk-PIC reconstruction employing the average mineral compositions from this study, combined with the average modal mineral abundances of PIC rocks from Grégoire et al. (2002; Appendix C); (C) Whole-rock compositions of orangeites (Becker and le Roex, 2006), lamproites (Rock, 1991), ultramafic lamprophyres (aillikites; Tappe et al., 2006), and kamafugites (Tappe et al., 2003), compared to the average MARID and PIC bulk-rock reconstructions from this study.

recalculation accounts for some discrepancies, particularly in Zr-Hf and the HREE (Fig. 10a).

In contrast, the average reconstructed bulk-MARID composition from this study is broadly similar to published bulk-rock trace element analyses of MARID samples (Grégoire et al., 2002; Waters, 1987a; Appendix C; Supplementary Table 1). However, the reconstructed average bulk-MARID composition displays lower abundances of some incompatible trace elements relative to previous data (particularly U, Sr, P, LREE; Fig. 10b).

The discrepancies in the abundances of some major (e.g., Ca) and trace (Th-U-P-LREE) elements between previous bulk-rock analyses and the bulk-MARID and -PIC reconstructions performed in this study for the same samples may relate to the petrographic heterogeneity in the portions of samples analysed in this study, compared to those available to Waters (1987a). However, it is also likely that these discrepancies can be attributed to the incorporation of secondary late-stage phases (e.g., apatite, calcite) in bulk-rock analyses, which were not included in the reconstructions performed herein, but would have been unavoidable in previous bulk-rock analyses. These differences in composition clearly display the inaccuracies associated with XRF-based and solution-mode determinations of bulk-MARID and -PIC compositions, as previously noted for bulk-peridotite (e.g., Grégoire et al., 2003; Simon et al., 2007) and bulk-eclogite analyses (as summarised by Jacob, 2004). Hereafter, references to bulk-rock compositions are therefore only made to the reconstructed compositions determined in this study.

Primitive-mantle normalised bulk-MARID and -PIC compositions display positive Rb, Nb-Ta-K, Pb and Ti anomalies, and negative Th-U and P anomalies. Such pronounced anomalies are not observed in ultramafic potassic magmas such as orangeites or lamproites (Fig. 10c). MARID rocks contain higher abundances of all incompatible elements relative to PIC, except for Rb (MARID = 390 ppm; PIC = 720 ppm) and K (MARID = 7.9 wt% K_2O; PIC = 9.4 wt% K_2O). This difference is attributed to the higher average modal abundance of phlogopite in PIC samples, as well as the greater Rb content of PIC phlogopite (800 vs 570 ppm).

7. Discussion

Since the original classification of MARID rocks (Dawson and Smith, 1977), several studies have attempted to unravel MARID genesis by investigating MARID geochemistry and mineralogy (e.g., Grégoire et al., 2002; Konzett et al., 2014; Waters, 1987a). In contrast, PIC rocks were first described as a distinct lithology by Grégoire et al. (2002), owing to differences in mineral major and trace element compositions, as well as radiogenic isotope compositions. The data presented in this study broadly match the criteria presented by Grégoire et al. (2002), suggesting that MARID and PIC are distinct groups of phlogopite-rich, ultramafic mantle rock whose compositions are owed to differing genetic processes. Each PIC phase displays higher Mg#, as well as higher Al_2O_3-Cr_2O_3-Na_2O and HFSE contents, relative to its MARID counterpart (Appendix A; Figs. 4–8). Clinopyroxene compositions are particularly useful for distinguishing between MARID and PIC rocks, with MARID clinopyroxene also displaying higher CaO and REE contents (Fig. 8c), and PIC clinopyroxene containing higher concentrations of TiO_2 (Fig. 5b). The differing compositional systematics of MARID and PIC minerals (Figs. 4–8) are probably related to element substitution phenomena (e.g., Fe-Al substitution in phlogopite; e.g., Dawson and Smith, 1977), some of which (e.g., higher Na_2O-Al_2O_3 in PIC clinopyroxene; Fig. 5c–d; Appendix A; Fitzpayne et al., 2018) likely relate to the pressure at which these minerals crystallised (e.g., Blundy et al., 1995). In the following section, the mineral chemical data for PIC rocks are first discussed in the context of PIC genesis, before the composition and formation of MARID rocks is addressed.

7.1. Genesis of PIC rocks: extreme peridotite metasomatism?

PIC mineral compositions fall within the broad compositional ranges of minerals from variably metasomatised peridotites from the Kimberley and other southern African kimberlites (Figs. 4–7). PIC minerals can be interpreted as more extreme products of the metasomatic progression of Erlank et al. (1987; i.e., increasing abundance of metasomatic minerals, associated with increasing Fe-Ti and decreasing Al-Cr-Mg concentrations in phlogopite and clinopyroxene; Figs. 4, 5). Moreover, PIC mineral compositions do not resemble those of minerals derived from "veins" that may be related to mantle "pegmatites" in peridotites derived from the Bultfontein kimberlite (e.g., PIC phlogopite contains 1.4 ± 0.4 wt% TiO_2 vs. <1 wt% in vein micas; Jones et al., 1982). The mineral data in this study appear to be consistent with PIC rocks forming as the result of extensive, progressive metasomatic alteration of peridotites. The absence of K-richterite in PIC rocks suggests that this style of metasomatism could be more closely related to phlogopite peridotites (PP) than to phlogopite-K-richterite peridotites (PKP). The similarity between PIC and PP rocks is supported by mineral compositions, whereby PIC phlogopite and clinopyroxene compositions closely resemble PP and are unlike PKP mineral compositions (Erlank et al., 1987; Appendix A). PKP phlogopite and clinopyroxene are both enriched in SiO_2 and MgO and depleted in Al_2O_3 compared to PIC/PP

minerals (Supplementary Fig. 1). Alternatively, the absence of K-richterite may be indicative of PIC genesis at greater depth than PKP rocks, because phlogopite is more stable than K-richterite at higher pressure (e.g., Konzett et al., 2014; Sweeney et al., 1993; Waters, 1987a).

The composition of the PIC parental metasomatising agent can be estimated using published values for $^{cpx\text{-}melt}Kd_{Fe\text{-}Mg}$ $[(Fe/Mg)_{cpx}/(Fe/Mg)_{melt}]$. Dasgupta et al. (2009) suggested a $^{cpx\text{-}melt}Kd_{Fe\text{-}Mg}$ value of 0.62 for carbonatite melt, and we employ this value here owing to (i) previous suggestions that PIC samples are formed from kimberlite melts (Grégoire et al., 2002), and (ii) the similarity in composition between the melt composition used by Dasgupta et al. (2009) and the composition of primitive kimberlite melts (Soltys et al., 2018a). This calculation indicates that PIC clinopyroxene is in equilibrium with a melt with Mg# between 83.4 and 86.2, which overlaps with the Mg# for primitive kimberlite melts (83.4–84.4; Soltys et al., 2018a). This conclusion is further supported by independent equilibrium $^{cpx\text{-}ol}Kd_{Fe\text{-}Mg}$ values of ~1.11 ± 0.12 (Witt-Eickschen and O'Neill, 2005) that imply equilibrium between PIC clinopyroxene and olivine with $Fo_{89.5–92.2}$. This range is similar to the range of magmatic olivine in kimberlites ($Fo_{90.0–91.1}$: Soltys et al., 2018b).

7.2. Genesis of MARID rocks

The veins in sample AJE-319 are composed of a mineral assemblage similar to that of MARID and PIC rocks. The major and trace element compositions of minerals in these veins are within the ranges shown by MARID minerals (Figs. 4–8), indicating that these are discrete veins of MARID material. Hereafter, this sample is included in discussions regarding MARID formation.

Previous studies of MARID xenoliths have presented conflicting interpretations concerning their genesis (e.g., Dawson and Smith, 1977; Grégoire et al., 2002; Sweeney et al., 1993; Waters, 1987a, 1987b). In the following section, we discuss our new mineral chemical data to evaluate the models of MARID genesis, starting with the magmatic model, which has been favoured by a majority of authors (e.g., Dawson and Smith, 1977; Erlank et al., 1987; Waters, 1987a).

7.2.1. Are MARID rocks magmatic cumulates/veins?

The veined textures in some composite MARID-peridotite samples (e.g., Fig. 2c) could be indicative of MARID formation from magmatic crystallisation in the mantle, as suggested by Dawson and Smith (1977) and Waters (1987a). The simplest approach to test the magmatic model for MARID formation is to compare the bulk-rock compositions of MARID samples to published ultramafic potassic magma compositions. Reconstructed bulk-MARID major element compositions from this study most closely resemble olivine lamproite bulk compositions (Appendix C, D). This may support the inference of Waters (1987a) that MARID rocks are the products of high-pressure crystallisation of lamproitic melts in the lithospheric mantle. However, the trace element patterns of reconstructed bulk-MARID rocks show large positive anomalies in Nb-Ta and Ti that are not present in mantle-derived magmas, including lamproites (Fig. 10c; Appendix C, D). The Nb-Ta-Ti enrichments of MARID rocks could be produced via:

(i) accumulation of HFSE-rich minerals (i.e. rutile, ilmenite) in an open system; or
(ii) extreme mineral-melt partition coefficients for the HFSE.

Even when the Monte Carlo simulations performed in this study include 0 vol% rutile and/or ilmenite, reconstructed bulk-rock trace element patterns retain their Nb-Ta and Ti anomalies, due to the enrichment of these elements in MARID phlogopite (Fig. 7a). The Monte Carlo simulations therefore appear to preclude option (i). Option (ii) can also be ruled out, given that the partition coefficients between MARID minerals (including phlogopite) and "typical" alkaline mafic melts (e.g., Adam and Green, 2011; Foley and Jenner, 2004; Schmidt et al., 1999) are not sufficiently elevated to cause HFSE-enrichments in MARID phases, unless the parental melts also contain anomalously high concentrations of these elements. The only possible case for MARID formation as magmatic veins appears to be under broader open-system conditions than those given in option (i), whereby MARID crystallisation was accompanied by the removal of a HFSE-depleted fluid/melt. The lack of a correlation between the K/Na ratios of MARID bulk-rocks and MARID K-richterite (Supplementary Fig. 2), for example, supports the widely-held view that MARID rocks crystallised under open-system conditions (e.g., Banerjee et al., 2018; Konzett et al., 1997; Tappe et al., 2006). Using published values of $^{cpx\text{-}melt}Kd_{Fe\text{-}Mg}$ (0.27 ± 0.03 for alkali basalt; Mollo et al., 2013), the melt in equilibrium with MARID clinopyroxene analysed in the current study must have Mg# between 51 and 77. The dissimilarity of this range compared to reconstructed bulk-MARID values (84.6 ± 5.2; this study) further supports the argument for open-system crystallisation of MARID rocks. In the following section, we assume that MARID rocks are formed by crystallisation of a melt. MARID genesis by progressive metasomatism is discussed thereafter.

We can investigate the potential interaction between MARID (and their parental melt) and surrounding peridotites by examining the compositions of minerals in the composite xenolith AJE-319. Olivine (Mg# = 88.0 ± 0.1) and clinopyroxene (Mg# = 90.9 ± 0.3) in sample AJE-319 imply a $^{cpx\text{-}ol}Kd_{Fe\text{-}Mg}$ of 0.73 ± 0.03, which is significantly different from the value of Witt-Eickschen and O'Neill (2005; $^{cpx\text{-}ol}Kd_{Fe\text{-}Mg}$: 1.11 ± 0.12), and implies chemical disequilibrium between MARID veins and the peridotite host of sample AJE-319. A similar $^{cpx\text{-}ol}Kd_{Fe\text{-}Mg}$ value (0.76) was observed in coexisting olivine and clinopyroxene in a sample containing both olivine and MARID minerals (Dawson and Smith, 1977). In sample AJE-319, no textural or chemical evidence for peridotite modification (e.g., olivine zonation) was observed next to the MARID veins. Diffusion of Mg-Fe or chemical exchange with the peridotite host therefore do not appear to play a role in MARID mineral composition, since MARID clinopyroxene in sample AJE-319 has not re-equilibrated with the surrounding mantle (represented by dunite). Consequently, it appears that the mineral Mg# in MARID samples can be used to examine the composition of the parental MARID melt.

The wide range of melt Mg# (51–77), which was calculated above based on MARID clinopyroxene Mg# (81–92), is likely to be due to different processes, including assimilation of mantle material, partial subsolidus re-equilibration between clinopyroxene that crystallised from the melt and minerals in the pre-existing mantle peridotite, melt mixing, melt differentiation, or some combination thereof. The first two of these possibilities can probably be discounted, on the basis that there is no unambiguous evidence in sample AJE-319, or any other composite MARID-peridotite xenolith (Boyd, 1990; Waters et al., 1989), that MARID-derived fluids are responsible for changes in peridotite mineral composition, or vice versa. The variations in clinopyroxene Mg# observed in MARID samples from this study cannot be easily related to clinopyroxene trace element patterns or ratios (Fig. 9a). This makes melt mixing an unlikely cause of clinopyroxene Mg# variations. However, extensive fractional crystallisation of the parental MARID melt remains a possible explanation for the range in MARID clinopyroxene and bulk-rock Mg# values, potentially in combination with wall-rock assimilation and/or melt mixing.

The removal of olivine from a parental orangeite (Sweeney et al., 1993) or silicate melt would be unlikely to affect the incompatible trace element composition of the melt, but must affect melt Mg#. In contrast, the removal of a carbonate-rich component would probably decrease the concentrations of REEs and increase the HFSE content of the remaining melt, owing to their relative compatibilities in carbonatite melts (Rudnick et al., 1993; Yaxley et al., 1998). However, Fig. 9a shows that La/Zr ratios (i.e. REE/HFSE) in MARID clinopyroxene are not correlated with Mg#, suggesting that fractional crystallisation

of both olivine and carbonates (or immiscible separation of a carbonatite melt) cannot be responsible for ranges in MARID mineral compositions, contrary to the proposal of Sweeney et al. (1993). Reconstructed whole-rock abundances of incompatible elements such as Th, U, and P are also not correlated with reconstructed bulk-MARID Mg# (Supplementary Fig. 3), further indicating that magmatic differentiation alone cannot explain MARID genesis. Additionally, bulk-rock Re-Os and zircon U-Pb ages for MARID samples indicate that MARID rocks could be formed much earlier (up to 170 Ma; Giuliani et al., 2015; Hamilton et al., 1998; Konzett et al., 1998, 2000; Pearson et al., 1995) than the earliest occurrence of orangeites in the Kimberley-Barkly West area (128 Ma; e.g., Smith et al., 1985), ruling out the requirement that MARID rocks formed by processes related to Cretaceous orangeite magmatism (Sweeney et al., 1993).

Owing to the ultrapotassic (>4.95 wt% K_2O) and hydrous (2.4–4.0 wt% H_2O) composition of MARID bulk-rocks that has been reconstructed in this study, we suggest that MARID rocks could be produced by open-system crystallisation of an alkali-rich hydrous silicate melt in mantle veins. In this scenario, the compositional variations shown by MARID minerals and bulk-rock reconstructions probably require fractionation of MARID minerals (and possibly olivine), combined with wall-rock assimilation and/or melt mixing.

7.2.2. Do MARID rocks represent extensively metasomatised peridotites?

The differences in composition between MARID and PIC minerals presented in this study (Figs. 4–9) are congruent with the interpretation that MARID and PIC formation are caused by different metasomatic agents (Grégoire et al., 2002). Although the MARID mineral compositions determined in the current study mostly fit within previously published ranges, our new data also show partial compositional overlaps for phlogopite, K-richterite, and clinopyroxene in MARID with those from peridotites from the Kaapvaal craton (Figs. 4–7). Furthermore, the compositions of MARID phlogopite and clinopyroxene lie at the enriched end of the metasomatic trends proposed by Erlank et al. (1987; Figs. 4, 5). MARID K-richterite also contains more Fe and less Cr than peridotitic K-richterite (Fig. 5a), and MARID ilmenite contains less Mg (and more Fe) than peridotitic ilmenite (Fig. 6), which together suggest similar Fe-rich metasomatism to that proposed by Erlank et al. (1987). This evidence therefore opens the possibility that MARID rocks could be genetically linked to phlogopite K-richterite peridotites (PKP). However, this interpretation is at odds with the radiogenic isotope constraints noted by Grégoire et al. (2002) indicating that MARID and PIC rocks are formed by different metasomatic agents, i.e. PKP and MARID rocks cannot be members of the same metasomatic progression as PP and PIC rocks. If this is also correct, there must be two separate series of metasomatism (PKP-MARID and PP-PIC), perhaps occurring at different depths as proposed by Waters (1987b) and Waters and Erlank (1988).

In conclusion, the results and models presented in this study combined with previous observations do not preclude the derivation of MARID either from strongly metasomatised peridotites that are genetically related to PKP, or from veins produced by open-system crystallisation.

7.3. The relationship between MARID rocks and mantle-derived ultramafic potassic magmas

Foley (1992) developed a model for the derivation of ultrapotassic melts from the melting of veined, metasomatised lithospheric mantle. Since then, mantle sources containing MARID components have been invoked in the genesis of several types of intraplate ultramafic potassic magma (Davies et al., 2006; Giuliani et al., 2015; Matchan et al., 2009; Rosenthal et al., 2009; Tappe et al., 2008). Recent experimental studies have attempted to simulate the model of Foley (1992), and have shown that melts derived from a combined MARID-harzburgite source may resemble the major element compositions of anorogenic lamproites (Förster et al., 2017, 2018).

In order to determine whether MARID rocks are likely to contribute to ultramafic potassic magmatism, two quantitative models for MARID-derived melts have been performed and compared to published compositions for such magmas. Neither model addresses the major element contributions of any harzburgite (or peridotite) wall-rock, or the necessary addition of P_2O_5 or volatile species, such as CO_2, that are critical to the formation of ultramafic potassic magmas such as orangeites, and which cannot be exclusively derived from a MARID source (Giuliani et al., 2015).

7.3.1. Melts in equilibrium with MARID minerals

A commonly adopted approach to melt modelling is the application of mineral-melt partition coefficients to determine the composition of the liquid in equilibrium with a given mineral. Ranges in melt trace element composition were calculated by applying published mineral-melt partition coefficients for alkali basalts (clinopyroxene and ilmenite: Zack and Brumm, 1998), lamproites (K-richterite: Bottazzi et al., 1999; phlogopite: Schmidt et al., 1999; and clinopyroxene: Foley and Jenner, 2004; Schmidt et al., 1999), and basanites (mica and clinopyroxene: Adam and Green, 2011) to the corresponding ranges in MARID mineral trace element compositions collected in this study (Appendix A), and plotting the minimum, maximum, and average of all the results. Fig. 11 shows that the large compositional ranges of melts in equilibrium with MARID minerals encompass those of orangeites, ultramafic lamprophyres, and other mantle-derived potassic magmas. Phlogopite-melt partition coefficients, which cause the wide ranges in possible composition in Fig. 11b & c, appear to be the least reliable of the available data. This is attributed to the low concentrations of many of the trace elements concerned in phlogopite. However, the ranges in melt composition displayed in Fig. 11 are so wide that this model is an unsatisfactory way of confirming genetic links between MARID rocks and ultramafic potassic magmas.

7.3.2. Incongruent melting of MARID rocks

The average bulk-MARID composition and modal mineral proportions in Table 3 can also be combined with mineral-melt partition coefficients in ultramafic potassic magmas to calculate the composition of a melt generated from a MARID lithology during incongruent melting.

The experiments performed by Sweeney et al. (1993) allow some inferences to be drawn with respect to MARID modal mineral abundances during melting. The modal mineral abundances of the original (unmelted) MARID sample used by Sweeney et al. (1993) are 63.2% phlogopite, 16.0% K-richterite, 1.2% rutile, <1% ilmenite, and 19.6% clinopyroxene (Waters, 1987b). In the experiments of Sweeney et al. (1993), K-richterite undergoes incongruent melting at low degrees of partial melting following either of two reactions:

$$1krt \rightarrow 0.45\ opx + 0.24\ cpx + 0.31\ melt;\ or$$

$$1krt \rightarrow 0.31\ ol + 0.24\ cpx + 0.45\ melt.$$

The incompatible trace element budgets of olivine and/or orthopyroxene produced in the melt residue in this model are assumed to be negligible compared to the bulk MARID sample. In Sweeney et al.'s (1993) experiments, there is no indication that either phlogopite or clinopyroxene make any contribution to low-degree (2–5%) melts. The model presented here therefore assumes that MARID phlogopite and clinopyroxene are stable and retain their original trace element compositions during the early stages of bulk-MARID melting. Finally, this model assumes that all rutile and ilmenite is incorporated into the melt phase during low-degree melting, because no mention is made of the presence of rutile and ilmenite in the experimental melt residues of Sweeney et al. (1993). Consequently, the contributions of MARID minerals to an incongruent MARID-derived equilibrium ("batch") melt can be assessed using published mineral-melt coefficients. A brief summary of the method by which this model was performed is included in Appendix E.

Although several studies have calculated mineral-melt partition coefficients for MARID minerals in ultramafic potassic magmas (e.g., phlogopite and clinopyroxene in lamproites; Schmidt et al., 1999), no

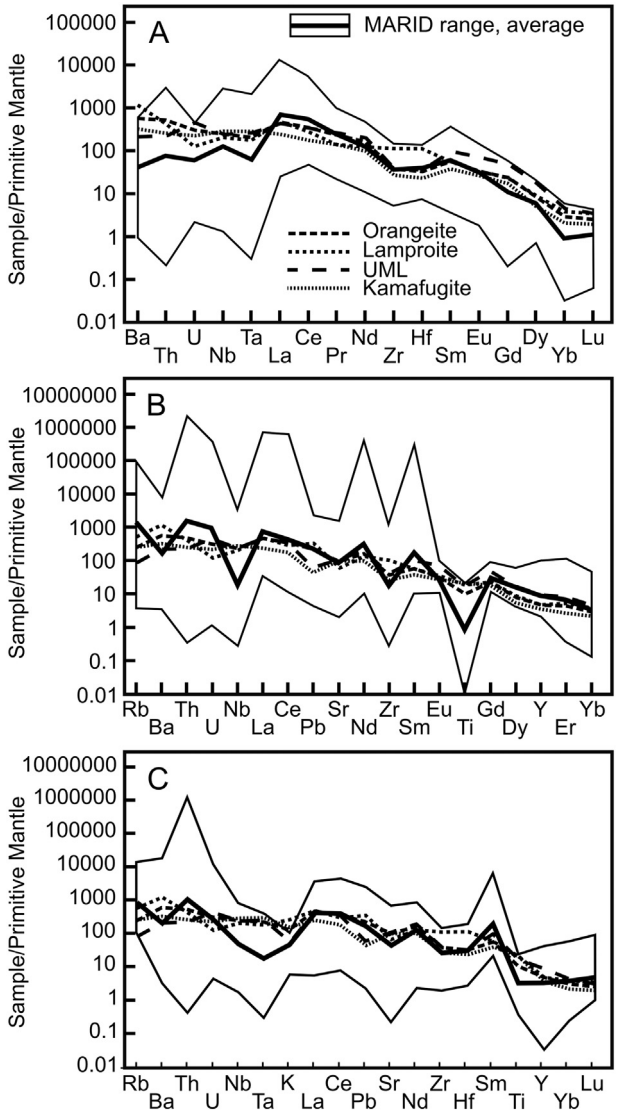

Fig. 11. Primitive mantle-normalised trace element diagrams comparing the compositions of melts in equilibrium with MARID minerals, which were calculated using published mineral-melt partition coefficients, to those of ultramafic potassic magmas (symbols as in Fig. 10c). Note different elements in each diagram, depending on elements studied by experimental studies. A: alkali basaltic melt in equilibrium with MARID clinopyroxene and ilmenite, using partition coefficients from Zack and Brumm (1998); B: lamproite melt in equilibrium with MARID clinopyroxene, phlogopite, and K-richterite, employing partition coefficients from Bottazzi et al. (1999), Foley and Jenner (2004), and Schmidt et al. (1999); C: basanite melt in equilibrium with MARID clinopyroxene and phlogopite, using partition coefficients from Adam and Green (2011); normalising values from McDonough and Sun (1995).

Table 3
Average MARID and PIC reconstructed bulk-rock compositions determined in this study.

	Bulk-MARID	Bulk-PIC		Bulk-MARID	Bulk-PIC
Mineral modal abundances (%)			Trace elements/ppm		
Phlogopite	71.3 ± 27.3	91.2 ± 7.1	Li	5.3 ± 1.9	2.6 ± 0.6
K-richterite	19.0 ± 26.8	n/a	B	2.2 ± 0.2	2.4 ± 0.2
Rutile	0.9 ± 1.5	0.02	P	22.3 ± 19.2	18.4 ± 3.4
Ilmenite	2.5 ± 2.5	0.6 ± 0.5	Sc	11.3 ± 6.9	6.1 ± 3.9
Clinopyroxene	6.3 ± 8.7	8.2 ± 7.0	Cu	2.2 ± 1.8	1.1 ± 0.5
			Zn	61.3 ± 13.6	32.5 ± 1.3
			Rb	386.2 ± 126.7	717.5 ± 141.3
Major elements/wt%			Sr	194.5 ± 185.2	24.0 ± 19.5
SiO_2	43.34 ± 2.76	41.88 ± 1.31	Y	0.91 ± 1.21	0.50 ± 0.5
TiO_2	4.50 ± 2.44	1.97 ± 0.57	Zr	57.1 ± 58.3	22.5 ± 15.4
Al_2O_3	7.14 ± 2.57	10.83 ± 1.35	Nb	177.8 ± 232.2	19.9 ± 8.3
Cr_2O_3	0.28 ± 0.15	0.37 ± 0.07	Mo	0.18 ± 0.15	0.04 ± 0.04
FeO^T	7.07 ± 2.33	4.10 ± 0.29	Ba	415.7 ± 273.4	159.3 ± 19.6
MnO	0.06 ± 0.02	0.03 ± 0.01	La	2.2 ± 2.8	0.41 ± 0.37
MgO	21.86 ± 1.85	24.13 ± 0.57	Ce	7.2 ± 9.5	1.6 ± 1.7
CaO	3.35 ± 2.03	1.98 ± 1.74	Pr	1.2 ± 1.5	0.29 ± 0.34
Na_2O	0.80 ± 0.80	0.31 ± 0.07	Nd	4.7 ± 6.3	1.5 ± 1.7
K_2O	7.94 ± 1.59	9.41 ± 0.83	Sm	0.82 ± 1.1	0.36 ± 0.42
F	0.28 ± 0.10	0.30 ± 0.08	Eu	0.22 ± 0.27	0.11 ± 0.12
Cl	0.03 ± 0.01	0.03 ± 0.01	Gd	0.60 ± 0.76	0.29 ± 0.32
H_2O	3.26 ± 0.51	3.59 ± 0.34	Dy	0.29 ± 0.36	0.16 ± 0.16
			Er	0.11 ± 0.12	0.05 ± 0.04
			Yb	0.07 ± 0.07	0.03 ± 0.02
			Lu	0.014 ± 0.010	0.006 ± 0.010
			Hf	2.1 ± 2.0	1.1 ± 0.7
			Ta	5.9 ± 6.2	1.7 ± 0.8
			Tl	1.0 ± 0.7	0.39 ± 0.03
			Pb	1.3 ± 0.7	0.32 ± 0.29
			Th	1.6 ± 1.6	0.08 ± 0.13
			U	0.19 ± 0.14	0.014 ± 0.010

All uncertainties are external 1 s.d., based on the average composition of each sample (see text); the average bulk-PIC** composition (Fig. 11) is not included here, but is presented in Appendix B.

work has been conducted on the full MARID suite of minerals under identical P-T-x conditions. Pilet et al. (2011) modelled alkaline magma formation by melting of amphibole-rich veins in the lithosphere, employing partition coefficients from several sources for all phases that occur in MARID and PIC rocks. The mineral-melt partition coefficients for rutile, ilmenite and clinopyroxene from Pilet et al. (2011) were therefore used for the incongruent melting model (Table 4). However, the model of Pilet et al. (2011) implies that all of the REE are more compatible in amphibole than in clinopyroxene, whereas clinopyroxene is the dominant REE host in MARID rocks (Figs. 7, 8; Appendix A). Similarly, the phlogopite-melt partition coefficients in Pilet et al. (2011) imply that the LREE are almost as compatible in phlogopite as they are in clinopyroxene, and that Sr is much more compatible in phlogopite than clinopyroxene, both of which are unlikely to be true given the trace element compositions of these minerals in MARID rocks (Figs. 7, 8; Appendix A). Therefore, phlogopite- and amphibole-melt partition coefficients were calculated by combining mineral-mineral partition coefficients from Grégoire et al. (2000; Table 4), who studied alkaline melt metasomatism in amphibole-bearing peridotite xenoliths, with mineral-melt partition coefficients in Pilet et al. (2011).

Fig. 12 shows the trace element compositions of the modelled MARID-derived melts for 2% and 5% melt fractions, compared to various ultramafic potassic magma compositions. This model demonstrates that low-degree, incongruent melting of MARID rocks broadly reproduces the trace element patterns of the magmas shown. However, relative to the published magma compositions, the modelled MARID-derived melts appear to be depleted in the REEs. The additional REE-rich and volatile components of these magmas might be supplied by melting of apatite and carbonates; however, the sources of these mineral phases (e.g., infiltrating carbonate-rich fluids; cf. Tappe et al., 2008) have not been considered in this model. Although both the melting models presented herein come with certain assumptions and caveats, they both appear to confirm previous suggestions that ultramafic potassic magmas may be derived from melting of MARID-rich portions of the mantle (e.g., Foley, 1992).

8. Conclusions

This study presents a large suite of mineral major and trace element compositions, as well as reconstructed whole-rock major and trace

Table 4
Mineral/melt partition coefficients employed in this study.

	Phlogopite/melt[a]	Amphibole/melt[b]	Rutile/melt[c]	Ilmenite/melt[c]	Clinopyroxene/melt[c]
Rb	2.24	0.044	0.01	0.004	0.0007
Ba	0.204	0.00887	0.01	0.007	0.00068
Th	0.000004	0.000044	0.5	0.008	0.0008
U	0.000016	0.000025	0.5	0.027	0.0008
Nb	0.301378	0.144	83.4	13.3	0.0077
La	0.0001608	0.040	0.3	0.01	0.0536
Ce	0.0001716	0.043	0.25	0.013	0.0858
Pb	0.014	0.00704	0.22	0.93	0.01
Sr	0.065	0.151	0.15	0.04	0.13
Nd	0.00057	0.041	0.1	0.03	0.19
Zr	0.00372	0.012	5.95	0.02	0.12
Hf	0.00858	0.051	7.08	0.08	0.26
Sm	0.00232	0.097	0.08	0.06	0.29
Eu	0.0047	0.096	0.05	0.14	0.47
Gd	0.0072	0.153	0.04	0.14	0.48
Er	0.00975	0.152	0.015	0.27	0.39
Yb	0.01505	0.119	0.012	0.19	0.43
Lu	0.0215	0.126	0.01	0.18	0.43

[a] Mineral/melt partition coefficients calculated using phlogopite-clinopyroxene partition coefficients in Grégoire et al. (2000) and clinopyroxene-melt coefficients of Pilet et al. (2011); partition coefficients in Pilet et al. (2011) are calculated from a compilation for minerals and a variety of alkaline magmas (e.g., basanites); see text for explanation.
[b] Mineral/melt partition coefficients calculated using phlogopite-amphibole partition coefficients given in Grégoire et al. (2000), and phlogopite-melt partition coefficients calculated in this study (i.e. see first column); see text for explanation.
[c] Mineral/melt partition coefficients in Pilet et al., 2011.

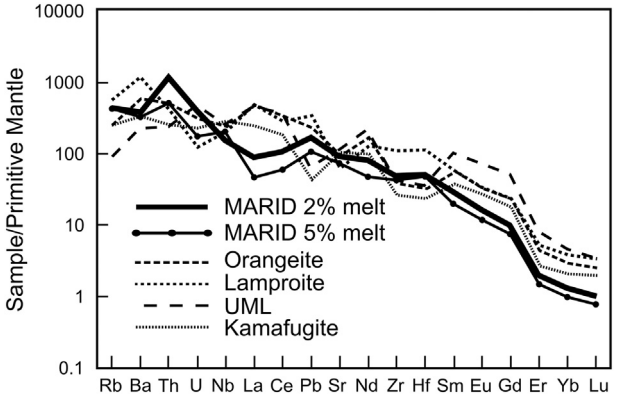

Fig. 12. Primitive mantle-normalised trace element diagram comparing the calculated compositions of 2% and 5% MARID-derived, equilibrium non-modal melts; the compositions of ultramafic potassic magmas from Fig. 10c are also plotted for reference, using the same line styles; normalising values from McDonough and Sun (1995).

element compositions, for MARID and PIC rocks from the Kimberley and Barkly West areas of South Africa. The new mineral chemical data support previous suggestions that PIC rocks are formed by intense peridotite metasomatism due to kimberlite melts. The MARID mineral major element compositions presented here exhibit wider ranges than previously reported. Although there is evidence to suggest MARID rocks may be formed by crystallisation from a fractionating melt, it has not been possible to rule out the contrasting model that MARID rocks form by metasomatism of peridotites caused by alkali-rich, hydrous silicate melts.

Melt modelling based on mineral trace element concentrations indicates that low-degree (≤5%) partial melting of MARID-rich sources may reproduce the trace element compositions exhibited by intraplate ultramafic potassic magmas such as orangeites, lamproites, and ultramafic lamprophyres. Future work combining the data presented herein with the radiogenic isotope compositions of MARID and PIC minerals from the same samples will help to elucidate the fundamental sources of MARID-PIC metasomatising agents, and provide more robust constraints on the origins of mantle-derived ultramafic potassic magmatism.

Supplementary data to this article can be found online at https://doi.org/10.1016/j.lithos.2018.08.036.

Acknowledgements

We acknowledge the support of Graham Hutchinson during SEM and EPMA sessions, and Alan Greig for his help with LA-ICP-MS analyses. We also thank De Beers Consolidated Mines, the University of Cape Town, John Gurney and Simon Shee for access to the samples examined in this study, and Jock Robey for invaluable support during field work in the Kimberley area. We thank Andrew Kerr for his efficient editorial handling of this manuscript. Finally, we would like to thank Michel Grégoire, Sebastian Tappe, Dmitri Ionov, Sally Gibson and two anonymous reviewers for their comments on this and a previous version of this manuscript. AG acknowledges funding from the Australian Research Council through a DECRA fellowship (grant no. DE-150100009). AF's PhD research is supported by a Gilbert Rigg scholarship from the University of Melbourne. This is publication 36 from the Kimberlites and Diamonds Research Group at the University of Melbourne (https://kimberlitesdiamonds.org/), also listed as contribution 1200 from the ARC Centre of Excellence for Core to Crust Fluid Systems (www.ccfs.mq.edu.au) and 1250 from the GEMOC Key Centre (www.gemoc.mq.edu.au).

References

Adam, J., Green, T., 2011. Trace element partitioning between mica-and amphibole-bearing garnet lherzolite and hydrous basanitic melt: 2. Tasmanian Cainozoic basalts and the origins of intraplate basaltic magmas. Contrib. Mineral. Petrol. 161 (6), 883–899.
Allsopp, H., Barrett, D.R., 1975. Rb-Sr age determination on South African kimberlite pipes. Physics and Chemistry of the Earth. 9, pp. 605–617.
Aulbach, S., O'Reilly, S.Y., Griffin, W.L., Pearson, N.J., 2008. Subcontinental lithospheric mantle origin of high niobium/tantalum ratios in eclogites. Nature 1, 468–472.
Aulbach, S., O'Reilly, S.Y., Pearson, N., 2011. Constraints from eclogite and MARID xenoliths on origins of mantle Zr/Hf-Nb/Ta variability. Contrib. Mineral. Petrol. 162 (5): 1047–1062. https://doi.org/10.1007/s00410-011-0639-y.
Banerjee, S., Kyser, T.K., Mitchell, R., 2015. Nitrogen isotopic compositions and concentrations in MARID xenoliths. Chem. Geol. 391, 83–89.
Banerjee, S., Kyser, T.K., Mitchell, R., 2018. Oxygen and hydrogen isotopic composition of phlogopites and amphiboles in diamond-bearing kimberlite hosted MARID xenoliths: constraints on fluid-rock interaction and recycled crustal material in the deep continental lithospheric mantle. Chem. Geol. 479, 272–285.
Becker, M., le Roex, A.P., 2006. Geochemistry of South African on- and off-craton, group I and group II kimberlites: petrogenesis and source region evolution. J. Petrol. 47 (4): 673–703. https://doi.org/10.1093/petrology/egi089.

Blundy, J.D., Falloon, T.J., Wood, B.J., Dalton, J.A., 1995. Sodium partitioning between clinopyroxene and silicate melts. J. Geophys. Res. 100 (B8), 15501–15515.
Bottazzi, P., Tiepolo, M., Vannucci, R., Zanetti, A., Brumm, R., Foley, S.F., Oberti, R., 1999. Distinct site preferences for heavy and light REE in amphibole and the prediction of $^{Amph/L}D_{REE}$. Contrib. Mineral. Petrol. 137, 36–45.
Boyd, F.R., 1990. Mantle metasomatism: evidence from a MARID-harzburgite compound xenolith. Carnegie Institute Washington Yearbook. 90, pp. 18–23.
Carswell, D., Clarke, D., Mitchell, R., 1979. The petrology and geochemistry of ultramafic nodules from Pipe 200, northern Lesotho. The Mantle Sample: Inclusions in Kimberlites and Other Volcanics, pp. 127–144.
Dasgupta, R., Hirschmann, M.M., McDonough, W.F., Spiegelman, M., Withers, A.C., 2009. Trace element partitioning between garnet lherzolite and carbonatite at 6.6 and 8.6 GPa with applications to the geochemistry of the mantle and of mantle-derived melts. Chem. Geol. 262, 57–77.
Davies, G.R., Stolz, A.J., Mahotkin, I.L., Nowell, G.M., Pearson, D.G., 2006. Trace element and Sr-Pb-Nd-Hf isotope evidence for ancient, Fluid-dominated enrichment of the source of Aldan shield lamproites. J. Petrol. 47 (6):1119–1146. https://doi.org/10.1093/petrology/egl005.
Dawson, J.B., Smith, J.V., 1977. The MARID (mica-amphibole-rutile-ilmenite-diopside) suite of xenoliths in kimberlite. Geochim. Cosmochim. Acta 41, 309–333.
van der Meer, Q.H., Klaver, M., Waight, T.E., Davies, G.R., 2013. The provenance of sub-cratonic mantle beneath the Limpopo Mobile Belt (South Africa). Lithos 170, 90–104.
Erlank, A., Waters, F., Hawkesworth, C., Haggerty, S., Allsopp, H., Rickard, R., Menzies, M., 1987. Evidence for mantle metasomatism in peridotite nodules from the Kimberley pipes, South Africa. Mantle Metasomatism, pp. 221–311.
Field, M., Stiefenhofer, J., Robey, J., Kurszlaukis, S., 2008. Kimberlite-hosted diamond deposits of southern Africa: a review. Ore Geol. Rev. 34 (1), 33–75.
Fitzpayne, A., Giuliani, A., Phillips, D., Hergt, J., Woodhead, J.D., Farquhar, J., Fiorentini, M.L., Drysdale, R.N., Wu, N., 2018. Kimberlite-related metasomatism recorded in MARID and PIC mantle xenoliths. Mineral. Petrol. 1–14.
Foley, S., 1992. Vein-plus-wall-rock melting mechanisms in the lithosphere and the origin of potassic alkaline magmas. Lithos 28 (3–6):435–453. https://doi.org/10.1016/0024-4937(92)90018-t.
Foley, S.F., Jenner, G.A., 2004. Trace element partitioning in lamproitic magmas – the Gaussberg olivine leucitite. Lithos 75, 19–38.
Förster, M.W., Prelević, D., Schmück, H.R., Buhre, S., Veter, M., Mertz-Kraus, R., Foley, S.F., Jacob, D.E., 2017. Melting and dynamic metasomatism of mixed harzburgite + glimmerite mantle source: implications for the genesis of orogenic potassic magmas. Chem. Geol. 455, 182–191.
Förster, M.W., Prelević, D., Schmuck, H.R., Buhre, S., Marschall, H.R., Mertz-Kraus, R., Jacob, D.E., 2018. Melting phlogopite-rich MARID: lamproites and the role of alkalis in olivine-liquid Ni-partitioning. Chem. Geol. 476, 429–440.
Giuliani, A., Phillips, D., Fiorentini, M.L., Kendrick, M.A., Maas, R., Wing, B.A., Woodhead, J.D., Bui, T.H., Kamenetsky, V.S., 2013. Mantle oddities: a sulphate fluid preserved in a MARID xenolith from the Bultfontein kimberlite (Kimberley, South Africa). Earth Planet. Sci. Lett. 376:74–86. https://doi.org/10.1016/j.epsl.2013.06.028.
Giuliani, A., Phillips, D., Kamenetsky, V.S., Kendrick, M.A., Wyatt, B.A., Goemann, K., Hutchinson, G., 2014. Petrogenesis of mantle polymict breccias: insights into mantle processes coeval with kimberlite magmatism. J. Petrol. 55 (4):831–858. https://doi.org/10.1093/petrology/egu008.
Giuliani, A., Phillips, D., Woodhead, J.D., Kamenetsky, V.S., Fiorentini, M.L., Maas, R., Soltys, A., Armstrong, R.A., 2015. Did diamond-bearing orangeites originate from MARID-veined peridotites in the lithospheric mantle? Nat. Commun. 6. https://doi.org/10.1038/ncomms7837.
Giuliani, A., Phillips, D., Kamenetsky, V.S., Goemann, K., 2016. Constraints on kimberlite ascent mechanisms revealed by phlogopite compositions in kimberlites and mantle xenoliths. Lithos 240-243:189–201. https://doi.org/10.1016/j.lithos.2015.11.013.
Grégoire, M., Moine, B., O'Reilly, S.Y., Cottin, J., Giret, A., 2000. Trace element residence and partitioning in mantle xenoliths metasomatized by highly alkaline, silicate-and carbonate-rich melts (Kerguelen Islands, Indian Ocean). J. Petrol. 41 (4), 477–509.
Grégoire, M., Bell, D., le Roex, A., 2002. Trace element geochemistry of phlogopite-rich mafic mantle xenoliths: their classification and their relationship to phlogopite-bearing peridotites and kimberlites revisited. Contrib. Mineral. Petrol. 142 (5):603–625. https://doi.org/10.1007/s00410-001-0315-8.
Grégoire, M., Bell, D., le Roex, A., 2003. Garnet lherzolites from the Kaapvaal craton (South Africa): trace element evidence for a metasomatic history. J. Petrol. 44 (4), 629–657.
Grégoire, M., Tinguely, C., Bell, D., le Roex, A., 2005. Spinel lherzolite xenoliths from the Premier kimberlite (Kaapvaal craton, South Africa): nature and evolution of the shallow upper mantle beneath the Bushveld complex. Lithos 84 (3), 185–205.
Hamilton, M.A., Pearson, D.G., Stern, R.A., Boyd, F.R., 1998. Constraints on MARID petrogenesis: SHRIMP II U-Pb zircon evidence for pre-eruption metasomatism at Kampfersdam. Paper Presented at the 7th International Kimberlite Conference, Extended Abstracts, Cape Town.
Hin, R., Morel, M., Nebel, O., Mason, P., van Westrenen, W., Davies, G., 2009. Formation and temporal evolution of the Kalahari sub-cratonic lithospheric mantle: Constraints from Venetia xenoliths, South Africa. Lithos 112, 1069–1082.
Jacob, D.E., 2004. Nature and origin of eclogite xenoliths from kimberlites. Lithos 77, 295–316.
Jochum, K.P., Weis, U., Stoll, B., Kuzmin, D., Yang, Q., Raczek, I., Jacob, D.E., Stracke, A., Birbaum, K., Frick, D.A., Günther, D., Enzweiler, J., 2011. Determination of reference values for NIST SRM 610-617 glasses following ISO guidelines. Geostand. Geoanal. Res. 35 (4), 397–429.
Jones, A.P., Smith, J., Dawson, J.B., 1982. Mantle metasomatism in 14 veined peridotites from Bultfontein Mine, South Africa. J. Geol. 435–453.
Katayama, I., Suyama, Y., Ando, J.-i., Komiya, T., 2009. Mineral chemistry and P–T condition of granular and sheared peridotite xenoliths from Kimberley, South Africa: Origin of the textural variation in the cratonic mantle. Lithos 109 (3–4):333–340. https://doi.org/10.1016/j.lithos.2008.05.004.
Konzett, J., Sweeney, R.J., Thompson, A.B., Ulmer, P., 1997. Potassium amphibole stability in the upper mantle: an experimental study in a peralkaline KNCMASH system to 8.5 GPa. J. Petrol. 38 (5), 537–568.
Konzett, J., Armstrong, R.A., Sweeney, R.J., Compston, W., 1998. The timing of MARID metasomatism in the Kaapvaal mantle: an ion probe study of zircons from MARID xenoliths. Earth Planet. Sci. Lett. 160 (1–2), 133–145.
Konzett, J., Armstrong, R.A., Günther, D., 2000. Modal metasomatism in the Kaapvaal craton lithosphere: constraints on timing and genesis from U–Pb zircon dating of metasomatized peridotites and MARID-type xenoliths. Contrib. Mineral. Petrol. 139 (6), 704–719.
Konzett, J., Wirth, R., Hauzenberger, C., Whitehouse, M., 2013. Two episodes of fluid migration in the Kaapvaal Craton lithospheric mantle associated with cretaceous kimberlite activity: evidence from a harzburgite containing a unique assemblage of metasomatic zirconium-phases. Lithos 182-183:165–184. https://doi.org/10.1016/j.lithos.2013.10.005.
Konzett, J., Krenn, K., Rubatto, D., Hauzenberger, C., Stalder, R., 2014. The formation of saline mantle fluids by open-system crystallization of hydrous silicate-rich vein assemblages – evidence from fluid inclusions and their host phases in MARID xenoliths from the central Kaapvaal Craton, South Africa. Geochim. Cosmochim. Acta 147: 1–25. https://doi.org/10.1016/j.gca.2014.10.015.
Lazarov, M., Woodland, A.B., Brey, G.P., 2009. Thermal state and redox conditions of the Kaapvaal mantle: a study of xenoliths from the Finsch mine, South Africa. Lithos 112, 913–923.
Lloyd, F.E., Bailey, D.K., 1975. Light element metasomatism of the continental mantle: the evidence and the consequences. Phys. Chem. Earth 9, 389–416.
MacGregor, I.D., 1979. Mafic and ultramafic xenoliths from the Kao kimberlite pipe. The Mantle Sample: Inclusion in Kimberlites and Other Volcanics, pp. 156–172.
Matchan, E., Hergt, J., Phillips, D., Shee, S., 2009. The geochemistry, petrogenesis and age of an unusual alkaline intrusion in the western Pilbara craton, Western Australia. Lithos 112:419–428. https://doi.org/10.1016/j.lithos.2009.04.034.
Matson, D.W., Muenow, D.W., Garcia, M.O., 1986. Volatile contents of phlogopite micas from south African kimberlite. Contrib. Mineral. Petrol. 93, 399–408.
McDonough, W.F., Sun, S.-s., 1995. The composition of the Earth. Chem. Geol. 120, 223–253.
Mollo, S., Putirka, K., Misiti, V., Soligo, M., Scarlato, P., 2013. A new test for equilibrium based on clinopyroxene-melt pairs: clues on the solidification temperatures of Etnean alkaline melts at post-eruptive conditions. Chem. Geol. 352, 92–100.
Pearson, D.G., Shirey, S.B., Carlson, R.W., Boyd, F.R., Pokhilenko, N.P., Shimizu, N., 1995. Re-Os, Sm-Nd, and Rb-Sr isotope evidence for thick Archaean lithospheric mantle beneath the Siberian craton modified by multistage metasomatism. Geochim. Cosmochim. Acta 59 (5), 959–977.
Peterson, T.D., Le Cheminant, A.N., 1993. Glimmerite xenoliths in early Proterozoic ultrapotassic rocks from the Churchill Province. Can. Mineral. 31 (4), 801–819.
Pilet, S., Baker, M.B., Muntener, O., Stolper, E.M., 2011. Monte Carlo simulations of metasomatic enrichment in the lithosphere and implications for the source of alkaline basalts. J. Petrol. 52 (7–8), 1415–1422.
Rehfeldt, T., Jacob, D.E., Carlson, R.W., Foley, S.F., 2007. Fe-rich Dunite Xenoliths from South African Kimberlites: cumulates from Karoo Flood Basalts. J. Petrol. 48 (7): 1387–1409. https://doi.org/10.1093/petrology/egm023.
Rehfeldt, T., Foley, S.F., Jacob, D.E., Carlson, R.W., Lowry, D., 2008. Contrasting types of metasomatism in dunite, wehrlite and websterite xenoliths from Kimberley, South Africa. Geochim. Cosmochim. Acta 72 (23):5722–5756. https://doi.org/10.1016/j.gca.2008.08.020.
Richardson, S.H., Erlank, A.J., Hart, S.R., 1985. Kimberlite-borne garnet peridotite xenoliths from old enriched subcontinental lithosphere. Earth Planet. Sci. Lett. 75, 116–128.
Rock, N.M., 1991. Lamprophyres. Springer Science and Business Media.
le Roex, A., Class, C., 2016. Metasomatic enrichment of Proterozoic mantle south of the Kaapvaal Craton, South Africa: origin of sinusoidal REE patterns in clinopyroxene and garnet. Contrib. Mineral. Petrol. 171 (2), 1–24.
Rosenthal, A., Foley, S.F., Pearson, D.G., Nowell, G.M., Tappe, S., 2009. Petrogenesis of strongly alkaline primitive volcanic rocks at the propagating tip of the western branch of the East African Rift. Earth Planet. Sci. Lett. 284 (1–2):236–248. https://doi.org/10.1016/j.epsl.2009.04.036.
Rudnick, R.L., McDonough, W.F., Chappell, B.W., 1993. Carbonatite metasomatism in the northern Tanzanian mantle: petrographic and geochemical characteristics. Earth Planet. Sci. Lett. 114, 463–475.
Schmidt, K., Bottazzi, P., Vannucci, R., Mengel, K., 1999. Trace element partitioning between phlogopite, clinopyroxene and leucite lamproite melt. Earth Planet. Sci. Lett. 168 (3), 287–299.
Shee, S.R., 1985. The Petrogenesis of the Wesselton Mine Kimberlites, Kimberley, Cape Province, R. S. A. (Ph.D.). University of Cape Town.
Simon, N.S.C., Irvine, G.J., Davies, G.R., Pearson, D.G., Carlson, R.W., 2003. The origin of garnet and clinopyroxene in "depleted" Kaapvaal peridotites. Lithos 71 (2–4):289–322. https://doi.org/10.1016/s0024-4937(03)00118-x.
Simon, N.S.C., Carlson, R.W., Pearson, D.G., Davies, G.R., 2007. The origin and evolution of the Kaapvaal cratonic lithospheric mantle. J. Petrol. 48 (3), 589–625.
Skinner, E.M.W., Smith, C.B., Viljoen, K.S., Clark, T.C., 1994. The petrography, tectonic setting and emplacement ages of kimberlites in the south-western border region of the Kaapvaal craton, Prieska area, South Africa. Kimberlites, Related Rocks and Mantle Xenoliths. Proceedings of the Fifth International Kimberlite Conference, Special Publication. 92 (1), pp. 80–97.
Smith, C.B., 1983. Pb, Sr and Nd isotopic evidence for sources of southern African Cretaceous kimberlites. Nature 304, 51–54.

Smith, C.B., Allsopp, H., Kramers, J., Hutchinson, G., Roddick, J., 1985. Emplacement ages of Jurassic-Cretaceous South African kimberlites by the Rb-Sr method on phlogopite and whole-rock samples. S. Afr. J. Geol. 88 (2), 249–266.

Soltys, A., Giuliani, A., Phillips, D., 2018a. A new approach to reconstructing the composition and evolution of kimberlite melts: a case study of the archetypal Bultfontein kimberlite (Kimberley, South Africa). Lithos 304-307, 1–15.

Soltys, A., Giuliani, A., Phillips, D., 2018b. Crystallisation sequence and magma evolution of the De Beers dyke (Kimberley, South Africa). Mineral. Petrol. 1–16.

Stiefenhofer, J., Viljoen, K.S., Marsh, J.S., 1997. Petrology and geochemistry of peridotite xenoliths from the Letlhakane kimberlites, Botswana. Contrib. Mineral. Petrol. 127, 147–158.

Sweeney, R.J., Thompson, A.B., Ulmer, P., 1993. Phase relations of a natural MARID composition and implications for MARID genesis, lithospheric melting and mantle metasomatism. Contrib. Mineral. Petrol. 115 (2), 225–241.

Tappe, S., Foley, S., Pearson, D., 2003. The kamafugites of Uganda: a mineralogical and geochemical comparison with their Italian and Brazilian analogues. Period. Mineral. 72, 51–77.

Tappe, S., Foley, S.F., Jenner, G.A., Heaman, L.M., Kjarsgaard, B.A., Romer, R.L., Stracke, A., Joyce, N., Hoefs, J., 2006. Genesis of ultramafic lamprophyres and carbonatites at Aillik Bay, Labrador: a consequence of incipient lithospheric thinning beneath the North Atlantic Craton. J. Petrol. 47 (7), 1261–1315.

Tappe, S., Foley, S.F., Kjarsgaard, B.A., Romer, R.L., Heaman, L.M., Stracke, A., Jenner, G.A., 2008. Between carbonatite and lamproite—Diamondiferous Torngat ultramafic lamprophyres formed by carbonate-fluxed melting of cratonic MARID-type metasomes. Geochim. Cosmochim. Acta 72 (13):3258–3286. https://doi.org/10.1016/j.gca.2008.03.008.

Tappe, S., Pearson, G.D., Nowell, G., Nielsen, T., Milstead, P., Muehlenbachs, K., 2011. A fresh isotopic look at Greenland kimberlites: cratonic mantle lithosphere imprint on deep source signal. Earth Planet. Sci. Lett. 305, 235–248.

Tappe, S., Romer, R.L., Stracke, A., Steenfelt, A., Smart, K.A., Muehlenbachs, K., Torsvik, T.H., 2017. Sources and mobility of carbonate melts beneath cratons, with implications for deep carbon cycling, metasomatism and rift initiation. Earth Planet. Sci. Lett. 466, 152–167.

Viljoen, F., Dobbe, R., Smit, B., 2009. Geochemical processes in peridotite xenoliths from the Premier diamond mine, South Africa: evidence for the depletion and refertilisation of subcratonic lithosphere. Lithos 112, 1133–1142.

Wagner, C., Deloule, E., Mokhtari, A., 1996. Richterite-bearing peridotites and MARID-type inclusions in lavas from North Eastern Morocco: mineralogy and D/H isotopic studies. Contrib. Mineral. Petrol. 124, 406–421.

Wasch, L., van der Zwan, F.M., Nebel, O., Morel, M., Hellebrand, E., Pearson, D., Davies, G., 2009. An alternative model for silica enrichment in the Kaapvaal subcontinental lithospheric mantle. Geochim. Cosmochim. Acta 73 (22), 6894–6917.

Waters, F.G., 1987a. A suggested origin of MARID xenoliths in kimberlites by high pressure crystallization of an ultrapotassic rock such as lamproite. Contrib. Mineral. Petrol. 95 (4), 523–533.

Waters, F.G., 1987b. A Geochemical Study of Metasomatised Peridotite and MARID Nodules From the Kimberley Pipes, South Africa. (Ph.D.). University of Cape Town.

Waters, F.G., Erlank, A., 1988. Assessment of the vertical extent and distribution of mantle metasomatism below Kimberley, South Africa. J. Petrol. (1), 185–204.

Waters, F.G., Erlank, A.J., Daniels, L.R.M., 1989. Contact relationships between MARID rock and metasomatised peridotite in a kimberlite xenolith. Geochem. J. 23 (1), 11–17.

Winterburn, P.A., Harte, B., Gurney, J.J., 1990. Peridotite xenolith from the Jagersfontein kimberlite pipe: I. Primary and primary-metasomatic mineralogy. Geochim. Cosmochim. Acta 54 (2), 329–341.

Witt-Eickschen, G., O'Neill, H.S.C., 2005. The effect of temperature on the equilibrium distribution of trace elements between clinopyroxene, orthopyroxene, olivine and spinel in upper mantle peridotite. Chem. Geol. 221, 65–101.

Yaxley, G.M., Green, D.H., Kamenetsky, V., 1998. Carbonatite metasomatism in the southeastern Australian lithosphere. J. Petrol. 39 (11−12), 1917–1930.

Zack, T., Brumm, R., 1998. Ilmenite/liquid partition coefficients of 26 trace elements determined through ilmenite/clinopyroxene partitioning in garnet pyroxenites. Extended Abstracts of the 7th International Kimberlite Conference, Cape Town, pp. 986–988.